UPPSALA
UNIVERSITET

Digital Comprehensive Summaries of Uppsala Dissertations from the Faculty of Science and Technology 1289

Haptics with Applications to Cranio-Maxillofacial Surgery Planning

PONTUS OLSSON

ACTA
UNIVERSITATIS
UPSALIENSIS
UPPSALA
2015

ISSN 1651-6214
ISBN 978-91-554-9339-4
urn:nbn:se:uu:diva-262378

Dissertation presented at Uppsala University to be publicly examined in 2247, Lägerhyddsvägen 2, Building 2, Uppsala, Friday, 16 October 2015 at 10:00 for the degree of Doctor of Philosophy. The examination will be conducted in English. Faculty examiner: Professor Blake Hannaford (University of Washington, USA).

Abstract
Olsson, P. 2015. Haptics with Applications to Cranio-Maxillofacial Surgery Planning. *Digital Comprehensive Summaries of Uppsala Dissertations from the Faculty of Science and Technology* 1289. 79 pp. Uppsala: Acta Universitatis Upsaliensis. ISBN 978-91-554-9339-4.

Virtual surgery planning systems have demonstrated great potential to help surgeons achieve a better functional and aesthetic outcome for the patient, and at the same time reduce time in the operating room resulting in considerable cost savings. However, the two-dimensional tools employed in these systems today, such as a mouse and a conventional graphical display, are difficult to use for interaction with three-dimensional anatomical images. Therefore surgeons often outsource virtual planning which increases cost and lead time to surgery.

Haptics relates to the sense of touch and haptic technology encompasses algorithms, software, and hardware designed to engage the sense of touch. To demonstrate how haptic technology in combination with stereo visualization can make cranio-maxillofacial surgery planning more efficient and easier to use, we describe our haptics-assisted surgery planning (HASP) system. HASP supports in-house virtual planning of reconstructions in complex trauma cases, and reconstructions with a fibula osteocutaneous free flap including bone, vessels, and soft-tissue in oncology cases. An integrated stable six degrees-of-freedom haptic attraction force model, *snap-to-fit*, supports semi-automatic alignment of virtual bone fragments in trauma cases. HASP has potential beyond this thesis as a teaching tool and also as a development platform for future research.

In addition to HASP, we describe a surgical bone saw simulator with a novel hybrid haptic interface that combines kinesthetic and vibrotactile feedback to display both low frequency contact forces and realistic high frequency vibrations when a virtual saw blade comes in contact with a virtual bone model.

We also show that visuo-haptic co-location shortens the completion time, but does not improve the accuracy, in interaction tasks performed on two different visuo-haptic displays: one based on a holographic optical element and one based on a half-transparent mirror.

Finally, we describe two prototype hand-worn haptic interfaces that potentially may expand the interaction capabilities of the HASP system. In particular we evaluate two different types of piezo-electric motors, one walking quasi-static motor and one traveling-wave ultrasonic motor for actuating the interfaces.

Keywords: medical image processing, haptics, haptic rendering, haptic gripper, visuo-haptic co-location, vibrotactile feedback, surgery simulation, virtual surgery planning, cranio-maxillofacial surgery

Pontus Olsson, Department of Information Technology, Division of Visual Information and Interaction, Box 337, Uppsala University, SE-751 05 Uppsala, Sweden.

© Pontus Olsson 2015

ISSN 1651-6214
ISBN 978-91-554-9339-4
urn:nbn:se:uu:diva-262378 (http://urn.kb.se/resolve?urn=urn:nbn:se:uu:diva-262378)

To my family

List of Papers

This thesis is based on the following papers, which are referred to in the text by their Roman numerals.

I **Olsson, P**., Nysjö, F., Rodríguez-Lorenzo, A., Thor, A., Hirsch, J.M., Carlbom, I.B. (2015) Haptics-Assisted Virtual Planning of Bone, Soft Tissue, and Vessels in Fibula Osteocutaneous Free Flaps, *Plastic and Reconstructive Surgery, Global Open*, 3(8).

II **Olsson, P**., Nysjö, F., Hirsch, J.M., Carlbom, I.B. (2013) A Haptics-Assisted Cranio-Maxillofacial Surgery Planning System for Restoring Skeletal Anatomy in Complex Trauma Cases, *Intl. J. Computer Assisted Radiology and Surgery*, 8(6), pp. 887-894.

III **Olsson, P**., Nysjö, F., Singh, N., Thor, A., Carlbom, I.B. (2015) Visuohaptic Bone Saw Simulator: Combining Vibrotactile and Kinesthetic Feedback. To appear in *Proc. ACM SIGGRAPH Asia*, Kobe, Japan.

IV **Olsson, P**., Nysjö, F., Hirsch, J.M., Carlbom, I.B. (2013) Snap-to-fit, a Haptic 6 DOF Alignment Tool for Virtual Assembly, *Proc. IEEE World Haptics Conference* (WHC), Daejeon, Korea, pp. 205-210.

V **Olsson, P**., Nysjö, F., Carlbom, I.B., Johansson, S. (2015) Comparison of Walking and Traveling-Wave Piezoelectric Motors as Actuators in Kinesthetic Haptic Devices. Manuscript for journal publication.

VI **Olsson, P**., Johansson, S., Nysjö, F., and Carlbom, I.B. (2012) Rendering Stiffness with a Prototype Haptic Glove Actuated by an Integrated Piezoelectric Motor, *Proc. Euro Haptics Conference*, Tampere, Finland, pp. 361-372.

VII **Olsson, P**., Nysjö, F., Seipel, S., Carlbom, I.B. (2012) Physically Co-Located Haptic Interaction with 3D Displays, *Proc. IEEE Haptics Symposium*, Vancouver, Canada, pp. 267-272.

The author is the main contributor in the above papers. Reprints were made with permission from the respective publishers.

Related Work

In addition to the papers included in this thesis, the author has also written or contributed to the following publications:

1. Nysjö, F., **Olsson, P**., Hirsch, J.M., Carlbom, I.B. (2014) Custom Mandibular Implant Design with Deformable Models and Haptics, *Proc. Computer Assisted Radiology and Surgery Conference*, Fukuoka, Japan, pp 246-247.
2. **Olsson. P**., Nysjö F., Aneer, B., Seipel, S., Carlbom, I.B. SplineGrip - An Eight Degrees-of-Freedom Flexible Haptic Sculpting Tool (2013), *ACM SIGGRAPH Posters*, Anaheim, USA, p. 50.
3. Nyström, I., **Olsson, P**., Nysjö, J., Nysjö, F., Malmberg, F., Seipel, S., Hirsch, J.M., Carlbom, I.B. (2015) Virtual Cranio-Maxillofacial Surgery Planning with Stereo Graphics and Haptics, Book Chapter, *Computer-Assisted Musculoskeletal Surgery*, Springer, Switzerland.
4. Carignan C., **Olsson P**., Tang J. (2005) Cooperative Control of Virtual Objects using Haptic Teleoperation over the Internet, *Intl. J. Disability and Human Development,* 4(4), pp. 261-268.
5. Tang, J., Carignan, C., **Olsson, P**. (2006) Tandem canoeing over the internet using haptic feedback, *Proc. IEEE 14th Symposium on Haptic Interfaces for Virtual Environment and Teleoperator Systems*, pp. 281-285.
6. **Olsson, P**., Nysjö, F., Johansson, S., Carlbom, I.B. (2011) Whole Hand Haptics, Medicinteknikdagarna, Linköping. (Abstract).
7. Hirsch, J.M., **Olsson, P**., Nysjö, F., Carlbom, I.B. (2014) A Stereo Haptics-Assisted Cranio-Maxillofacial Surgery Planning System for Restoring Skeletal Anatomy in Complex Reconstructive Procedures, Bernd-Spiessl-Symposium, Basel. (Abstract).
8. Hirsch, J.M., **Olsson, P**., Nysjö, F., Carlbom, I.B. (2015) Wouldn't You Like to Plan Your Reconstructions in a 3D Virtual System in 30 Minutes and Operate Next Day? Surgery Planning with a Haptics-Assisted Surgery-Planning System (HASP), Bernd-Spiessl-Symposium, Basel. (Abstract).

Contents

Abbreviations

CMC	Carpometacarpal
CMF	Cranio-Maxillofacial
CT	Computed Tomography
DOF	Degrees of Freedom
DOFF	Degrees of Force Feedback
EM	Electromagnetic
fMRI	Functional Magnetic Resonance Imaging
FOFF	Fibula Osteocutaneous Free Flap
HASP	Haptics-Assisted Surgery Planning
HCI	Human Computer Interaction
HIP	Haptic Interface Point
HU	Hounsfield Units
ICP	Iterative Closest Point
MP	Metacarpophalangeal
MRI	Magnetic Resonance Imaging
OR	Operating Room
STP	Standard Temperature and Pressure
TWUM	Traveling-Wave Ultrasonic Motor
VSP	Virtual Surgery Planning
WIMP	Windows, Icons, Menus, and Pointer
WQSM	Walking Quasi-static Motor

1. Introduction

Increasing computational power and improving quality of imaging devices in combination with progress in image processing algorithms are paving the way for sophisticated surgery planning systems. Such systems have demonstrated great potential to help surgeons achieve a better functional and aesthetic outcome for the patient, and at the same time reduce time in the operating room resulting in considerable cost savings. However, the two-dimensional tools employed in these systems today, such as a mouse and a conventional graphical display, are difficult to use for interaction with three-dimensional anatomical images.

Haptics relates to the sense of touch, and *haptic technology* encompasses algorithms, software, and hardware designed to engage the sense of touch. In this thesis we explore the use of haptic technology in combination with stereo visualization to enhance the usability and efficiency of computer-assisted cranio-maxillofacial (CMF) surgery planning and training. We describes the development of our haptics-assisted surgery planning (HASP) system, as well as two prototype hand-worn haptic interfaces actuated by piezo-electric motors, which may potentially expand the haptic interaction capabilities of the HASP system. We also describe a novel hybrid haptic interface for surgical bone saw simulation. The development of a haptic system is a diverse challenge; this thesis comprises haptic rendering, system development, interaction design, and design and control of hardware.

The *contributions* section summarizes the publications that are the basis of this thesis, but we begin with an introduction to the various concepts, technologies, and methods used throughout the thesis.

2. Haptics

Haptics, from Greek: *haptesthai* (to contact, to touch), refers to interaction that involves the sense of touch. *Haptic* relates to touching as *visual* relates to seeing and *auditory* relates to hearing [1]. The field of haptics can be divided into the following sub-fields: *human haptics* refers to human sensing and manipulation through touch, *machine haptics* refers to the design and use of machines to stimulate the sense of touch, and *computer haptics* focuses on algorithms and software that simulate and render the feel of virtual objects, analogous to algorithms and software in *computer graphics* that render the visual appearance of virtual objects [2].

Ivan Sutherland realized the potential of incorporating multiple senses, including touch, for interaction with machines when he imagined the "Ultimate Display" in 1965 [3]. Despite the importance of touch in our everyday interaction with the surrounding physical world, computer scientists and researchers of human computer interaction (HCI) have mainly focused on visual, and to some extent, auditory interfaces. In traditional interfaces without haptic feedback, you may touch the *computer*, but the computer cannot touch *you*.

2.1 Human Haptics

Humans rely heavily on the sense of touch in everyday interaction with the surrounding physical world; consider for example the difficulty performing fine manipulation tasks such as tying your shoelaces, or exploring the roughness of a surface, with input from your visual sense alone. Klatzky and Lederman divide touch into *cutaneous*, *kinesthetic*, and *haptic systems* that are distinguished on the basis of the underlying neural inputs [4].

Cutaneous receptors are embedded in the skin and provide information about pressure, skin stretch, and vibration, including the subtle forces and skin displacements caused by light touch and fine textures against the skin, causing *tactile perception*. In glabrous (hairless) skin there are four types of cutaneous receptors that respond to mechanical stimulation. Meissner's cor-

puscles respond to light touch, Ruffini corpuscles detect strain deep into the skin, Merkel cells detect sustained pressure, and Pacinian corpuscles respond to vibrations [5, 6]; see Figure 1. Other receptors include *thermoreceptors* which respond to absolute and relative changes in temperature and *nociceptors* which respond to potentially damaging stimuli. Cutaneous receptors are distributed over the whole body in the skin, our largest organ. Sensitive areas, such as fingertips, are most densely populated [7]. During manipulation of objects, such as holding a glass of water, receptors in the fingertips provide information necessary to apply the right amount of force to keep the glass it in a stable grip, and avoid slipping [5].

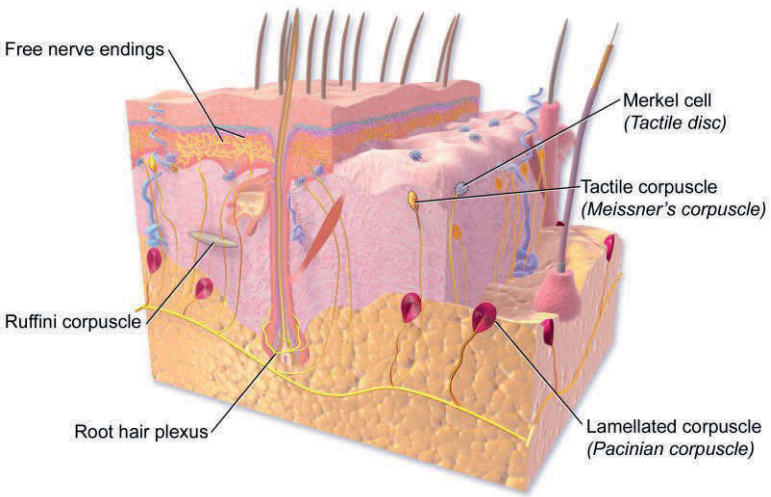

Figure 1. Cutaneous receptors in the skin.[1]

Kinesthetic receptors are located in tendons, muscles and joints and provide information about movements and articulation of our limbs. However, studies suggest that cutaneous receptors also contribute to kinesthetic perception [8, 9]. The human haptic system employs both cutaneous and kinesthetic receptors, but is associated with an active procedure, that is, when the sensory inputs are combined with a controlled body motion such as active exploration of an object.

Neural activity in response to touch stimuli can be studied by inserting a needle electrode into single nerves, and recording electrical impulses. This method, referred to as *microneurography*, was developed by Hagbarth and Vallbo in the 1960s [10]. They performed their first experiments on them-

[1] Image: *Tactile receptors* from Blausen Gallery 2014, Wikiversity Journal of Medicine. DOI:10.15347/wjm/2014.010. ISSN 20018762. Licensed under CC BY 3.0 / Cropped from original.

selves, but it has since become an established method for studying the relationships between different types of touch stimuli and activity in the different types of receptors.

Psychophysics is another area of human haptics that quantitatively investigates the relationship between physical stimuli and the perceptions they cause.

The *somatosensory cortex*, the main receptive area in the brain for the sense of touch, is located directly adjacent to the *motor cortex*, which controls the execution of movements. Since motor control and haptic perception are so tightly connected, haptics is sometimes referred to as a bi-directional sense.

2.2 Machine Haptics

Haptic devices, sometimes referred to as *haptic displays,* are human-machine interfaces, typically electro-mechanical, that mediate the human sense of touch. In robotics and tele-manipulation, such interfaces have existed since the 1950s [11]. Tele-robotic manipulators enable human operators to remotely manipulate hazardous or inaccessible environments in, for example, nuclear plants, oceans, and space. As these systems evolved, robotic manipulators were equipped with force sensors to sample contact forces at the remote environment. This force information is transferred and displayed to the human operator with specialized haptic display hardware enabling him or her to manipulate and "touch" objects remotely. Such haptic feedback facilitates manipulation, but presents technical challenges such as delay and stability of the force-feedback loop. Figure 2 shows an example of a tele-manipulation architecture with haptic feedback.

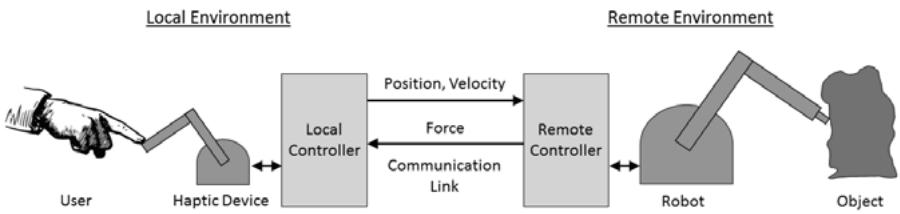

Figure 2. Tele-manipulation with force-feedback. The user may manipulate remote objects and, depending on the fidelity of the tele-manipulation system, perceive shape information, surface stiffness, and surface texture.

All haptic devices generate an output that can be perceived haptically. Some devices, but not all, also acquire information *from* a user. *Tactile* and *kinesthetic* haptic devices are used for the different parts of the haptic sense: Braille displays, which are used to display text for the visually impaired, is an example of a tactile display [12]. *Vibrotactile* displays generate vibrations in many gaming consoles and are a silent alternative to the auditory ringing signal in cellphones. Tactile displays are typically one-directional; they present information *to* a user, but do not contain sensors to acquire information *from* the user.

Kinesthetic devices on the other hand, are typically bi-directional. A common type of kinesthetic device is based on a mechanical linkage that resembles a robotic arm. A user interacts with the device by grasping and manipulating a handle, or *end-effector*, attached to the end of the arm. Sensors in the device track motion and/or forces applied to the handle, and integrated actuators generate force and/or torque feedback to the user. Such devices thus provide a bi-directional channel between the user and a virtual environment. Work-space size, number of degrees-of-freedom (DOF) and degrees-of-force-feedback (DOFF), maximum force and torque, and price varies greatly between different devices. Figure 3 shows examples of commercial haptic devices. The price range between the cheapest device shown here, the Novint Falcon at about $200, to the most expensive high-end device, the Phantom Premium, spans about two orders of magnitude.

Figure 3. Commercial haptic devices. From the left: Novint Falcon (three DOF, three DOFF); Phantom Omni (six DOF, three DOFF); Phantom Desktop (six DOF, three DOFF); Phantom Premium (six DOF, six DOFF).

The target application determines the requirements for a haptic device, which often become a trade-off between force, fidelity, number of DOF, complexity, and cost. If a high maximum force is important, strong mechan-

ical linkages and actuators are required which increase mass and inertia. In order to display remote or virtual objects realistically, the device must provide sufficient force, otherwise a stiff object does not feel stiff. It must also provide sufficient velocity, otherwise the user feels resistance when moving his or her fingers quickly, and the device must be able to move smoothly; force noise distorts the perception.

2.2.1 Causality

A kinesthetic haptic device is classified as an *impedance* or *admittance* device depending on whether it senses a position and a velocity from the user and responds with a force, or vice versa [13]. This is referred to as its *causality*. Impedance devices respond with force feedback based on position and/or velocity input. Such devices do not require force sensors, which makes their design relatively straightforward. They are typically *back-drivable*, meaning that they can be moved freely at low friction when their actuators are disengaged. Commercial devices are often of the impedance type.

Admittance devices, on the other hand, respond with position and/or velocity feedback to applied forces. They are generally non-back-drivable, and require a force sensor that samples applied forces [14]. The display of very stiff surfaces, critical in applications such as virtual assembly [15], is straightforward with an admittance device, as they can be programmed to respond with zero positional change when the user applies an increasing force towards a rigid virtual object, in contrast to impedance devices, where a change in force response is always preceded by some change in input position and/or velocity. Figure 4 illustrates the causality concept. The devices used in the surgery planning application described in Publications I and II are impedance devices, while the grippers described in Publications V and VI are admittance devices.

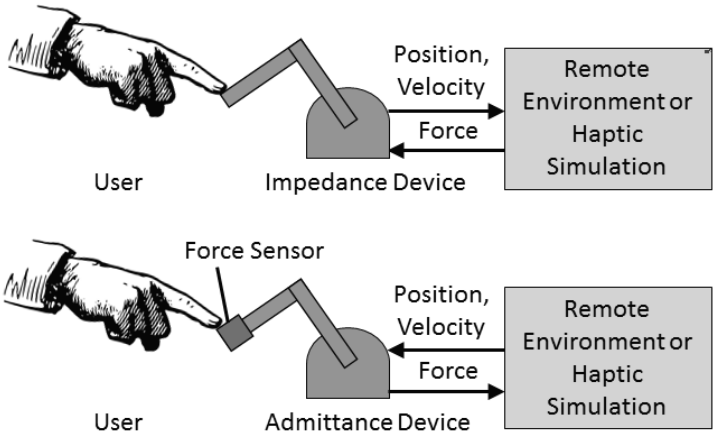

Figure 4. Impedance and admittance devices. Top: Impedance device. The user moves the handle of the device, which responds with force feedback. Bottom: Admittance device. The user applies force to a force sensor on the handle of the device, which responds with position and/or velocity feedback.

2.3 Computer Haptics

The possibility to simulate haptic properties of virtual environments emerged as computers became increasingly powerful. Massie and Salisbury [16] were pioneers in 1993 with a system where a kinesthetic haptic device sensed the 3D-position of a handle attached to a mechanical linkage, and transferred the position to a simulated, virtual environment. A real-time algorithm calculated forces based on the position of the handle; if it came in contact with a simulated object in the virtual environment, referred to as a *virtual object*, motors in the device exerted forces on the handle via the linkage. This enables users to explore and manipulate simulated virtual environments and objects with real-time haptic feedback. They subsequently developed their prototype into the Phantom, a well-known commercial haptic device [17].

Today, *visuo-haptic* systems that combine haptic and visual feedback are very common; see Figure 5. In these systems, the haptic and graphic rendering typically run in parallel in separate *threads*. The haptic thread reads positional and rotational input from a haptic device, renders contact forces (and sometimes torque), and sends force and torque information back to the device at a high rate, often 1 kHz. The graphic thread renders virtual objects visually at a lower rate. Often the graphic thread also renders a graphical probe, or *stylus*, that follows the motions of the haptic handle. Some systems, for example the SOFA framework [18], employ additional threads for

computationally intense dynamic simulations of for example soft tissue, an important component in surgical simulators.

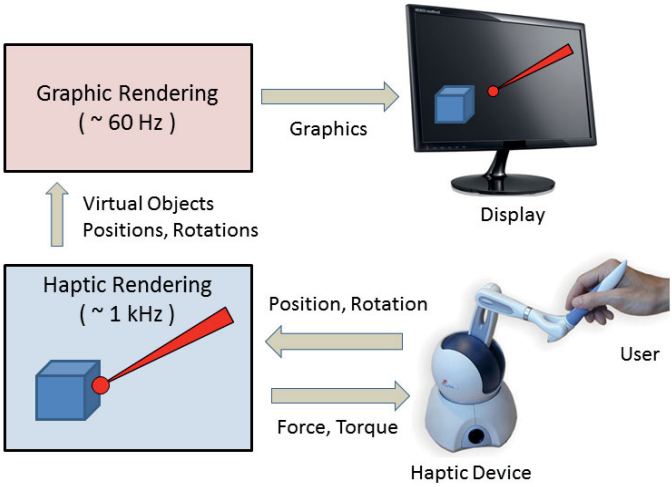

Figure 5. Visuo-haptic system with an impedance-type haptic device.

2.4 Haptic Rendering

Haptic rendering is the process of calculating forces to be displayed on a haptic device [19]. One may make the analogy to computer graphics, where rendering is the process of generating images of virtual objects for a visual display. Some haptic rendering algorithms are designed to generate forces based on the exploration of abstract information, but most algorithms render contact forces from geometric data [20]. The two main components of most contact rendering algorithms are collision detection and collision response. As the user manipulates the handle of a haptic device, the algorithm continuously acquires the position and orientation of the handle and detects collisions with virtual objects. If a collision occurs, the algorithm computes interaction forces based on predefined rules for collision response, and displays the forces to the user via the handle of the haptic device. Such a haptic loop gives an illusion of touching and interacting with virtual objects via a probe, or tool.

Great efforts have been made to improve haptic rendering algorithms for increased efficiency and realism [21]. A central challenge in the simulation and rendering of realistic force feedback is to maintain a high update rate. The update rate affects the maximum virtual object surface stiffness that can be rendered without instability in the force-feedback loop. Mark et al. [22] suggest using as much as 1 kHz, compared to 30–60 frames per second re-

quired to achieve smooth graphical update. Haptic rendering software requires a combination of highly optimized algorithms, carefully designed data structures, and pre-computation, in addition to large computational power to achieve a realistic haptic experience.

Several software frameworks implement haptic rendering algorithms, for example H3DAPI [23], Chai 3D [24], and SOFA [18].

2.4.1 Virtual Object Representation

Rendering of contact forces from interaction with virtual objects requires a suitable geometric representation of the objects. For objects with a very simple geometry such as spheres or cubes, or objects with a well-defined behavior, such as linear virtual springs, parametric descriptions may be preferable. In the evaluation of the haptic grippers in Publication V we employ virtual springs that are fully defined by a rest position and a stiffness parameter. For objects with complex geometry, a common approach familiar from computer graphics is to describe the surface of the virtual objects as a set of polygons with vertices and surface normals. Since only the surface is stored, the objects occupy relatively little data storage, which may be critical in applications with objects of very complex geometry. Polygonal representations are dominant in algorithms that are limited to rendering contact forces between a point or spherical probe that follows the endpoint of the haptic device's handle, the *Haptic Interface Point* (HIP), and the virtual objects [25, 26]. For distributed contact between surfaces of arbitrary geometry, not limited to points or spheres, representations such as the *Voxmap-Pointshell* are common.

The Voxmap-Pointshell class of algorithms described below employ, as the name suggests, a dual geometric representation [27, 28]. First, each object is described by a *voxmap*; a precomputed voxel-rasterized distance map that for all voxels within the object stores the closest distance to the surface. Often a computationally efficient estimate such as the 3-4-5 chamfer distance transform [29] works satisfactory. Second, each object is also represented by a *pointshell*; a set of approximately equidistant surface points, each with an associated surface normal. The required sampling resolution is highly application dependent and a tradeoff between detail and computational speed; in the surgery planning system described in Publications I and II, most virtual objects have sub-millimeter sized voxels. Figure 6 shows examples of objects defined parametrically, by polygons, and by a Voxmap-Pointshell representation. In addition to geometric information, other properties such as

surface stiffness, weight, and sometimes surface texture may be included in the object definition.

Figure 6. Virtual object representations. Left: Simple sphere defined by a radius, r. Center: Polygonal representation. Right: Voxmap-Pointshell representation. The red dots represent the pointshell, and the squares represent voxmap elements with intensities proportional to their distances from the object surface.

2.4.2 Three-DOF Rendering

The first haptic rendering algorithms for interaction with 3D geometric virtual objects were limited to three DOF Cartesian force feedback, i.e., a three dimensional force vector. In their simplest form, the user controls the position of a point-shaped probe, or HIP, via a haptic device. When pushed into a virtual object, the algorithm computes a 3D force vector directed towards the closest point on the object surface, with a magnitude proportional to the penetration depth; see Figure 7 (left).

Such *direct rendering* suffers from force direction ambiguity; when the user pushes the HIP past the center of an object, the HIP falls through the object, as the surface on the opposite side of the object becomes closer to the HIP than the entry surface; see Figure 7 (right). A common solution is to use a virtual coupling, as described below.

Due to numerical imperfections, the HIP sometimes falls though small gaps between the polygons that describe the virtual objects. The *Ruspini* rendering algorithm solves this by replacing the point shaped HIP with a sphere [26].

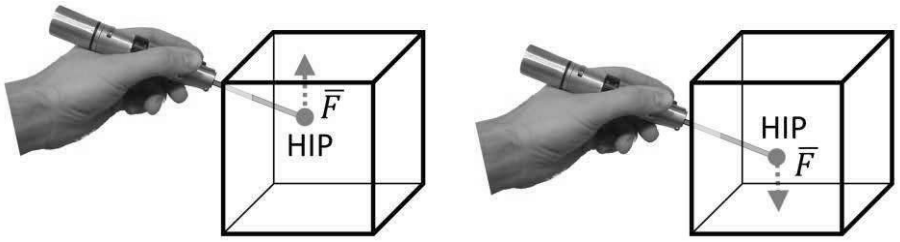

Figure 7. Three DOF direct haptic rendering. Left: The user pushes the HIP down into a cubical virtual object, and the rendering algorithm computes a force $\bar{F}$ from the HIP upwards towards the closest object surface. Right: If the user pushes the HIP further down into the object, the bottom side eventually becomes closer and the force flips direction, the HIP "pops though" the object.

2.4.3 Virtual Coupling

A common solution to avoid force ambiguity is to use an auxiliary object that always stays on the object surface, often referred to as a *proxy*, or *god-object* [25]. When the user pushes the HIP inside a virtual object, the proxy slides on the object surface towards the HIP. Between the proxy and the HIP is a virtual spring, a *virtual coupling*, that tries to push the device (at the HIP position) towards the proxy (at the surface), with a force magnitude proportional to their separation, see Figure 8. In six-DOF haptic rendering there are two separate three-DOF virtual coupling springs; one for linear translations that yields a Cartesian force, and one for rotations that yields a torque.

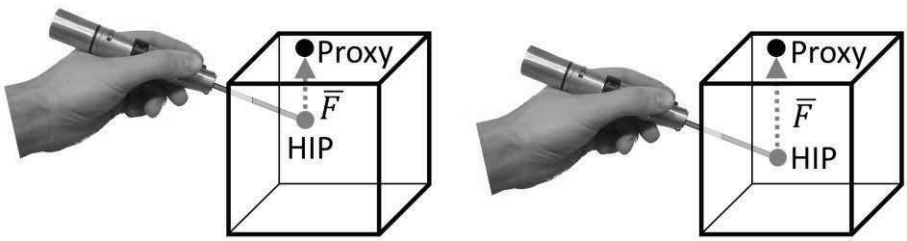

Figure 8. Rendering with proxy. Left: The user pushes the HIP down into a cubical virtual object, and the proxy remains on the top surface. The rendering algorithm computes a force $\bar{F}$ from the HIP upwards towards the proxy. Right: If the user pushes the HIP further down into the object, the proxy remains on the top surface, and $\bar{F}$ retains an upwards direction.

2.4.4 Six-DOF Rendering

In the real world, we do not often interact with the world via a point-shaped probe. And, contacts between objects rarely occur at a single point. Instead most contacts between objects are spatially distributed over surfaces of various shapes. For example, when an archeologist assembles a broken historical artifact, or when a surgeon assembles a fractured bone and searches for the optimal fit between two fragments, contact forces stem from distributed locations on the fracture surfaces, not from a single point; see Figure 9.

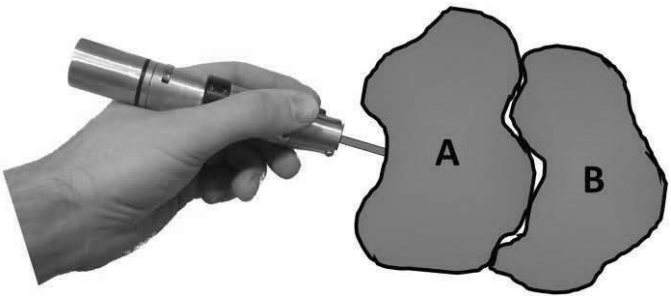

Figure 9. Distributed contact between two objects. Instead of a point or sphere-shaped HIP, the user here manipulates an arbitrarily shaped object (A) and pushes it in contact with a fixed object (B).

Haptic rendering of forces from the interaction between a grasped virtual object of arbitrary shape and a virtual environment is often referred to as six-DOF rendering, as it encompasses three DOF Cartesian force and three DOF torque. Displaying all six degrees of force feedback requires a device able to produce torque feedback in addition to Cartesian force feedback. Six-DOF rendering accommodates more realistic and versatile haptic interaction than simple contact rendering with points or spheres, and was first developed by McNeely et al. at Boeing in the late 90's for haptics-assisted virtual aircraft assembly and disassembly analysis [27]. Barbic [28] extended the method with deformable models. In Publications II we describe virtual bone fragment assembly where the fragments employ a dual Voxmap-Pointshell representation; the manipulated fragment employs a point-shell representation, all other bone structures are held fixed and use voxmap representations. The algorithm approximates distributed surface contacts by summing contact force and torque contributions from all pointshell points that are in contact with another virtual object.

Figure 10 shows a manipulated pointshell object (A) in contact with a fixed voxmap object (B). Each surface point in the pointshell that is in contact with the fixed object yields a force in the direction of the pointshell's inward

normal at the point. The force has a magnitude proportional to its penetration depth, which can quickly be found by retrieving the precomputed voxmap value at the point's position. Consider the point at (C). In addition to its contact force, it also yields torque based on force magnitude and the angle between the force direction and a lever vector (D) between the contact point and the point where the user grasped the object (E). The force and torque contributions from all points are summed at the grasp point. The manipulated object is connected to the HIP via one linear and one rotational spring. In each haptic frame, the object is moved and rotated such that it reaches a force and torque equilibrium between contact and spring forces. This is referred to as a *quasi-static virtual coupling* [30]. In Publications I and II we use such coupling for stability, and to limit penetrations between bone fragments.

In Publication IV, we augment the six-DOF contact rendering and quasi-static virtual coupling with a six-DOF attraction force based on surface-matching: *Snap-to-fit*.

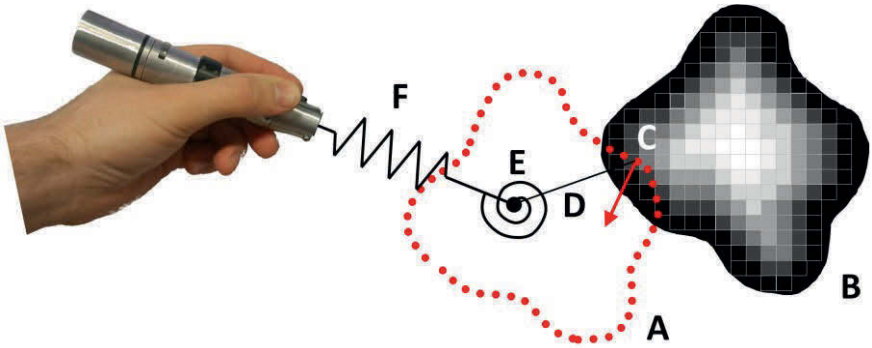

Figure 10. A manipulated object (A) in contact with a fixed object (B); point in contact (C); lever vector (D); grasp point (E); virtual coupling (F).

2.5 Actuation

Actuation is one of the major challenges in haptic devices, especially in hand-worn devices such as haptic grippers. Force-to-mass and force-to-volume ratios of the actuators are critical to prevent user fatigue, excessive device bulkiness, and inertia.

2.5.1 Electromagnetic Motors

Broadly speaking, *electromagnetic* (EM) motors generate force or torque from interaction between current-carrying conductors, typically arranged as coils, and a magnetic field. The current through the conductors constitute moving charges, thus the conductors are subject to the Lorentz force, $\boldsymbol{F}_{Lorentz} = \boldsymbol{i}l \times \boldsymbol{H}$, where $\boldsymbol{F}_{Lorentz}$ is the resulting force vector from a current $\boldsymbol{i}$ though a conductor of length l passing through a magnetic field $\boldsymbol{H}$.

EM motors are the most common actuators in kinesthetic haptic devices, as a result of their availability and relatively low price. Examples include the widely used Phantom devices [17], and many research and educational devices [31-33]. It is possible to drive EM motors with open-loop control because their produced force follows a predictable, nearly linear relationship to the driving current. Their low friction often allows the motor shaft to be freely moved when the motor is not actively driven. This makes them suitable for impedance control. Their main drawbacks are their relatively high mass-to-force ratio, and their need of reduction gearing to produce sufficient force in haptic applications; see Figure 11. Reduction gearing increases bulkiness, friction, and apparent inertia of the motor. If the reduction ratio becomes too large, the motor‘s back-drivability diminishes and the device requires force sensors and admittance control. Finally, EM motors are magnetic, and thus incompatible with magnetic resonance imaging (MRI) environments.

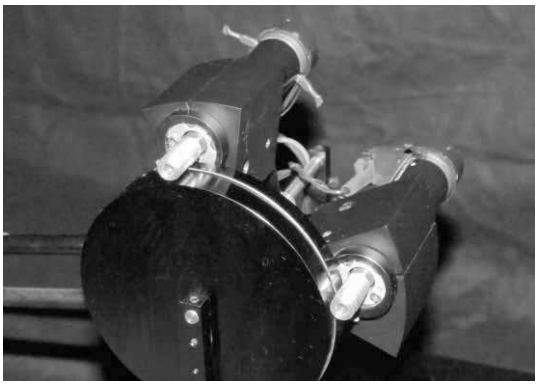

Figure 11. Two EM motors in a Phantom Premium device, with a classical capstan reduction for torque magnification: a wire along the circumference of the large wheel is wrapped around the motor pulleys. Such reduction minimizes backlash, but is often large and encumbering.

2.5.2 Piezoelectric Motors

Piezoelectricicity, from Greek: *piezin* (to press) was first described in a scientific publication by the brothers Jacques and Pierre Curie in 1880 [34]. The piezoelectric effect is the accumulation of electric charge in certain materials in response to mechanical stress. The reverse piezoelectric effect, the generation of stress in materials in response to an applied electrical field, is the basis for piezoelectric motors.

Two common piezoelectric motor types are the traveling-wave ultrasonic motor (TWUM) and the walking quasi-static motor (WQSM). Albeit rare compared to traditional EM motors, the TWUM is the most common piezoelectric motor in haptic interfaces. Examples include a hand exoskeleton with several DOFs described by Choi et al. [35], and a *functional magnetic resonance imaging* (fMRI)-compatible one-DOF interface described by Flueckiger et al. [36]. WQSM's for haptic interfaces are even rarer. In Publication VI, we explore using a WQSM as an actuator in a haptic gripper, and in Publication V we compare two haptic grippers, actuated by these two different piezoelectric motor types.

2.5.2.1 Traveling-Wave Ultrasonic Motors (TWUM)

TWUMs operate at ultrasonic frequencies close to mechanical resonance, above the limit of the human hearing. The active component of a TWUM is a ring-shaped stator with a friction layer with "teeth" on one side, and piezoelectric elements attached to the other side [37]. These elements are divided into separate electrode areas; see Figure 12.

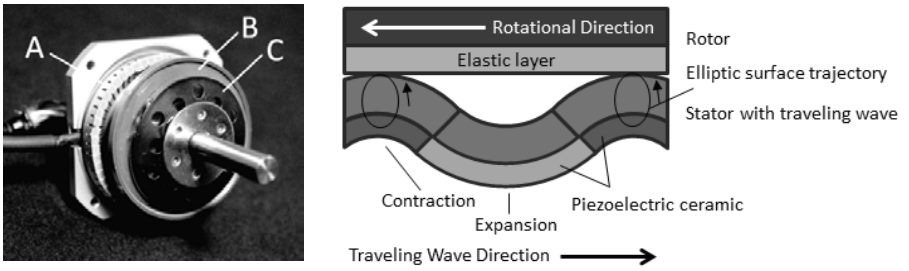

Figure 12. Left: Key components of a TWUM. Stator with teeth (A), rotor (B), and pre-load spring (C). The piezoelectric elements are attached to the stator backside (not visible in figure). Right: TWUM principle. Expansion and contraction of piezoelectric elements in the stator generates a traveling wave and the stator surface points follow elliptical trajectories, generating torque in the rotor by friction contact. The wave amplitude is exaggerated for illustration purposes.

When supplied by separate sinusoidal voltage signals, typically phase shifted by 90 degrees, a traveling flexural wave is generated in the stator ring (A). This wave motion drives by friction the rotor (B), which is preloaded by a strong spring (C) against the stator. Figure 12 (right) shows a schematic of the stator traveling wave driving the rotor where the contact points move along elliptical paths creating a rotation opposite to the traveling wave direction.

The motor operates close to its resonance frequency, and the torque and velocity can be adjusted by tuning the signal frequency in the vicinity of the resonance. The motor can also be controlled by the phase shift, the signal voltage amplitude, and/or the pulse length of the drive signals. Moving the frequency away from resonance, or moving the phase shift away from 90 degrees, decreases the velocity. The rotational direction of the motor is determined by the phase shift between the voltage sources. Compared to quasi-static motors described below, TWUMs' higher driving frequencies generally enable a higher maximum velocity.

2.5.2.2 Walking Quasi-Static Motors (WQSM)

Figure 13 (left) shows an example of a linear PiezoLEGS® LT2010 WQSM from Piezomotor AB [38]. These motors operate in an audible frequency range well below resonance, hence quasi-static. Two stators are pressed against a linear drive rod with leaf springs in a symmetric arrangement. The active parts in each stator are four piezoelectric legs that can be elongated and bent, making it possible to "walk" the rod by driving the legs in two pairs, 180 degrees out of phase; see Figure 13 (right).

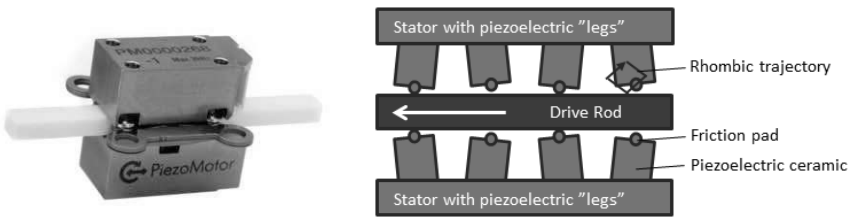

Figure 13. Left: PiezoLEGS® LT2010 WQSM. The leaf-springs, integrated with the visible attachment "ears", create a compressive force between the two stators and the white drive rod. Right: WQSM principle. The piezoelectric legs bend and extend depending on the drive signals to "walk" the drive rod. The leg motion is exaggerated for illustration purposes.

In the simplest case, the leg tip follows a rhombic trajectory and is in friction contact with the rod during the upper part of the rhomb while releasing and returning for the next step during the lower part of the rhomb. The drive rod is always in friction contact with at least two leg tips of each stator and, if the legs are not activated, the drive rod is held rigidly by the legs. If the load exceeds the holding force, the rod slips without motor damage. The positional precision is extremely high with fractional steps as short as a single nanometer [9], and the non-resonant operation offers a high max/min velocity ratio, where the lower velocity is limited only by the driving electronics. The driving frequency, which affects the motor velocity, is in the case of the WQSM in Figure 13 limited to about 3 kHz; higher frequencies may damage the motor.

2.6 Applications

Haptic technology has a wide range of applications. Examples include stroke rehabilitation [39], assembly and disassembly analysis [40], virtual design [41, 42], and of course, entertainment [43].

This thesis focuses on the medical field, where an important application area is skills training, in particular for surgical procedures [44], where a central research challenge is realistic simulation of tissue and organs. Surgery involves many manual tasks that require fine motor skills, and the operating room (OR) is the best place to learn. However, the number of times a surgical resident may have the opportunity to practice a procedure is limited; OR costs and patient safety concerns have resulted in less teaching in the OR during actual procedures [45]. Alternatives such as practicing surgical procedures on a cadaver are neither convenient nor cost effective. Plastic anatomical replicas can be used for practicing techniques such as osteotomies (bone cutting), but they do not offer a realistic operating experience. This motivates the use of simulation in surgical education [44]. Realistic simulation may help surgical trainees practice important technical skills through repetition. Haptics contributes significantly to realism in training simulators, as medical professional rely on their sense of touch for many procedures, including palpation [46], laparoscopic surgery [47], and needle insertion [48].

A number of research systems for virtual surgery planning have been proposed where haptic interfaces effectively replaces conventional interaction tools, such as a mouse and a keyboard, for interaction with three-

dimensional patient-specific anatomical images [49-51]. In these systems, the main purpose of the haptic feedback is to support planning tasks, for example finding a precise alignment for bone fragments in trauma cases. Here, realism may not be as central as in a surgery simulator. Useful, but non-realistic attraction forces that guide the fragment alignment, absent gravity which allows virtual bone fragments to be suspended in space, and artificial haptic constraints may be more important than realism. In Publication I and II we describe how haptics in combination with stereo visualization can make cranio-maxillofacial surgery planning more efficient and easier to use.

2.7 Haptic Grippers

Haptic grippers incorporate multiple-finger interaction and multiple points of contact with virtual objects in contrast to most kinesthetic haptic devices that restrict the user to interacting with a virtual world indirectly via a pencil-like handle or tool. Such indirect interaction works well for tasks that are performed with tools in the physical world, such as laparoscopic and endoscopic surgery; see Figure 14. Many haptic simulators for training such procedures have been proposed [47]. However, in our daily life, we are used to more dexterous interaction with the physical world using multiple fingers and points of contact for grasping, manipulation, and exploration of objects. Multiple points of contact increase our object identification ability; Jansson et al. demonstrated a significant increase in object identification efficiency when going from one to two finger exploration [52]. A mechanism able to increase the active DOFs of a commercial haptic device without significant increase in volume or weight would greatly benefit dexterous haptic virtual interaction.

Several approaches to multi-finger haptics have been proposed. Multiple one-point-of-contact devices may be combined to achieve multi-point interaction. For example, Ang et al. combine two Phantom Omni devices to provide a pinch-grip interface [53]. However, such combination limits the effective workspace to the intersection of the two devices' workspaces and introduces a risk for mechanical collisions.

Another approach is to transmit forces to the interface via for example steel wires in flexible housings (Bowden cables) from a remote actuator that could be placed on a desk, which reduces the requirement for low actuator mass and volume. The pinch-grip interface designed by Najdovski et al. [33], the

hand rehabilitation exoskeleton by Wang et al. [54], as well as the classical CyberGrasp interface [55] employ such remote actuation. The Rutgers Haptic Master II-ND [56] provides four actuated DOFs with remotely powered pneumatic pistons. In these systems, the mass of the complete actuator is not carried by the user, making its size and weight less critical. However, Bowden cables or pneumatic tubes limit the device's free movement. In addition, precise, stable control is difficult to achieve when dynamics such as friction, backlash, and inertia of the force transmission have to be considered.

Figure 14. Laparoscopic surgery.[2] The surgeons interact with the internal organs indirectly, via laparoscopic tools.

Figure 15. Connecting an exoskeleton haptic gripper to a mechanically grounded device enables the display of mass and inertia of grasped virtual objects. The brain is added artificially, for illustrative purposes.

[2] Photo: *Surgeons perform laparoscopic stomach surgery*, Samuel Bendet, US Air Force. Public Domain.

Haptic grippers implemented as actuated exoskeletons to be worn on the hand provide an unlimited workspace as the interface follows the motions of the hand, but requires a carefully selected actuation. Publication V and VI describe the design and evaluation of two haptic grippers actuated by two different piezo-electric motors; TWUM and WQSM, integrated directly into the exoskeleton. Since such devices are body-grounded, that is they are carried by the user rather than operated on a desk, the gripper must be attached to a mechanically grounded and actuated mechanical linkage if a haptic application requires the display of for example mass and inertia of a grasped virtual object. Such grounding limits the workspace of the gripper to that of the grounded device. Figure 15 shows the gripper described in Publication VI connected to a kinesthetic Phantom Premium device.

3. Medical Image Analysis

Digital images, in particular computed tomography (CT) images, are the main source of information in the surgery planning applications in this thesis. A two-dimensional digital image can be represented by a matrix, **M**[i, j], where the coordinates i and j correspond to locations within the image, and the matrix values correspond to local image properties such as image intensity, or, in the case of CT images, the attenuation of radiation in tissue. A two-dimensional image element is called a *pixel* and a volumetric three-dimensional image element is called a *voxel*.

The main task in *image analysis* is extraction of relevant information from digital images [57]. General applications are very diverse; examples include face recognition [58], hand-written text recognition [59], fingerprint analysis, materials science, security, and many more. A few examples from a vast variety of medical applications include automatic analysis of histopathological samples for malignancy grading [60, 61], virus detection in electron microscopy images [62], and vessel detection in computed tomography images [63].

3.1 Computed Tomography

Computed tomography (CT) is one of the most common 3D image modalities and provides the most detailed images of bony structures for diagnostic purposes. The technique is based on measuring transmission of X-rays from several different directions through an object of interest and reconstructing a three-dimensional image by filtered back-projection. The X-ray attenuation coefficients are typically transformed to absolute Hounsfield units (HU), where the radio-density of distilled water at standard temperature and pressure (STP) is defined as zero HU, and air as -1000 HU. In order to increase the contrast in blood vessels, a contrast agent may be injected into the patient's bloodstream prior to the scan. By precise timing of the deposit of the contrast agent and the scan, it is possible to optimize the contrast in a region of interest. Such images are referred to as *CT-angiograms*. In this thesis, all

volumetric anatomical images were derived from stacks of CT images or CT-angiograms; see Figure 16. Each slice in a stack constitutes a two-dimensional image, together they form a three-dimensional volumetric image, **M**[i, j, k]. The maximum CT resolution depends on the quality of the imaging device, the radiation exposure time, and the reconstruction algorithm. Figure 17 shows a case from Publication II where a voxel represents a volume with the dimensions 0.35 x 0.35 x 0.6 mm.

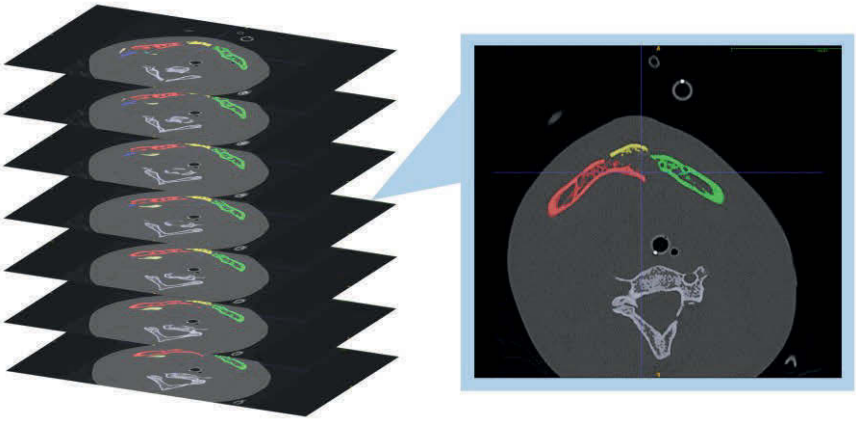

Figure 16. CT Images. Left: A stack of CT images from different cross-sections of a fractured mandible that together form a volumetric image. Right: One image from this stack, where individual bone fragments are segmented and visualized in unique colors.

3.2 Segmentation

A common task in image analysis is finding and delineating specific objects in images, a procedure referred to as *segmentation*. Objects of interest could be cells, internal organs, or other microscopic or macroscopic structures. In this thesis, we use segmented bony structures for reconstruction planning of trauma cases, and also soft tissue such as blood vessels for planning of oncology cases. A human user could manually delineate objects of interest in the images, but manual segmentation is often too tedious and time-consuming for routine clinical usage. In addition, by operating at a single slice at the time the user may not perceive the full 3D structure.

Computerized image segmentation is divided in a number of steps ranging from low-level identification of for example pixels (or voxels) within a predefined intensity range, or pixels on object boundaries with a high gradient

magnitude, to higher-level operations such as identification of a specific cell type or malignancy grading. Designing automatic and robust segmentation pipelines is a difficult task, and a very active area in image analysis research.

Semi-automatic or interactive segmentation methods combine interactive user input with algorithms to achieve accurate and repeatable segmentations. This type of methods can be a viable alternative if automatic segmentation fails and a limited amount of user-interaction time is acceptable. We employ a semi-automatic method called *BoneSplit*, described by Nysjö et al. [64] to segment bony structures in the images used in this thesis. The user begins by marking bone fragments of interest in unique colors with a tool that resembles a paintbrush; see Figure 17. The algorithm then delineates the individual fragments with a random-walks method, and the user may interactively adjust the result by adding or removing markers. To segment blood vessels for planning of oncology cases, the user first searches for vessels of interest by manually scrolling through a stack of CT-angiogram images. Once a vessel of interest is found, he or she places a starting point or *seed* within the vessel. We then use a tubular tracking algorithm described by Friman et al. [65] that searches for and delineates tubular structures that pass through the seed.

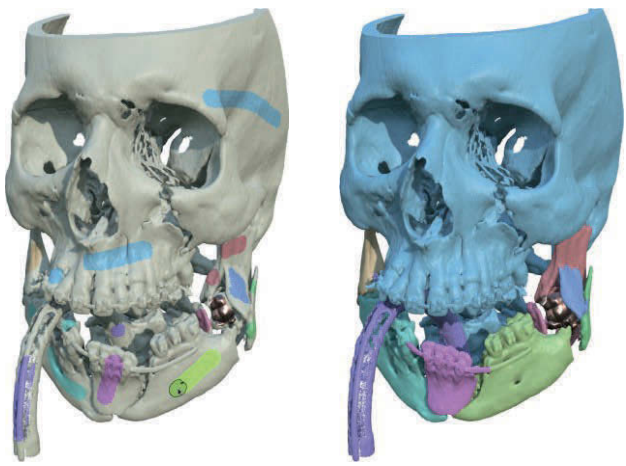

Figure 17. Segmentation with BoneSplit. Left: The user marks individual bone fragments in unique colors with a virtual paintbrush. Right: Segmentation result.

4. 3D Visualization and Display

Visualization refers to techniques and methods for visual data presentation [66]. With the high-performance computer graphics hardware and algorithms readily available today, two-dimensional (2D) data is relatively straightforward to present on a regular computer monitor; an everyday example is the display of digital photos. Data of higher dimensions however, require careful dimensionality reduction and projection while retaining as much relevant information as possible.

In surgery planning, the user typically views 3D volumetric images of anatomical regions derived from CT images. Traditional planning systems project this data onto a 2D plane, which can be displayed on a regular 2D computer monitor. Although visual cues such as perspective, shading, and shadows improve spatial comprehension, the planar format introduces a risk of ambiguity in spatial relations, which may be mitigated with a more sophisticated display technique, such as stereoscopy.

4.1 Stereoscopy

Stereoscopy, from Greek: *stereos* (solid) and *skopein* (watching), refers to techniques and methods to render and display 3D objects such that they can be perceived with binocular vision. Stereoscopic visualization has shown to aid surgeons orient in spatially complex anatomical regions [67]. This is important for CMF surgery planning, which requires high spatial precision and accuracy [68].

A variety of techniques are available to provide the user's left and right eye with correct stereo views [69]. A common approach utilizes glasses, either active or passive, to separate the views. *Shutter-glasses* yield brilliant colors and high resolutions at a fairly low cost. Such glasses generally use liquid crystal technology to alternate transparency between the left and right eye. A communication link synchronizes the glasses with the display to ensure that the correct image is shown for each eye. *Polarization glasses* are another option, commonly employed in 3D cinema. Here, two images are

displayed simultaneously with light in orthogonally polarized directions, which are separated by polarization filters in the glasses. In contrast to active shutter glasses, passive polarized stereo glasses do not require batteries or synchronization, and generally retain the brightness of the images better.

Auto-stereoscopic displays provide stereoscopy without headgear. One such display is the Holographic optical element (HOE), that acts as a projection screen for a number of projectors [70]. The HOE is made such that the image from each projector onto the holographic element can be viewed within a narrow angle representing one view of a 3D object; see Figure 18. With multiple, properly spaced, projectors each eye receives a separate view and the user perceives a 3D object in the space above the HOE. Other examples of auto-stereoscopic displays include lenticular sheet displays and parallax barrier displays [71].

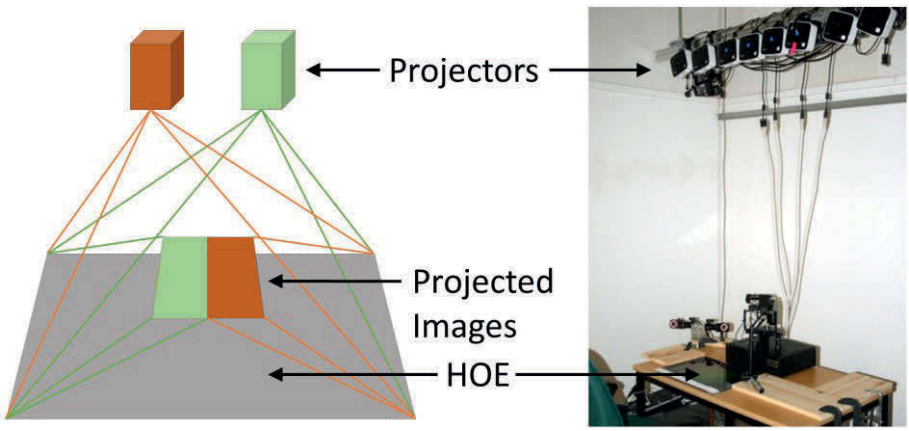

Figure 18. Left: Autostereoscopic Holographic Optical Element principle. Two (or more) projectors project images on the HOE. The HOE separates the projected images such that the image from the left projector can only be viewed by the right eye, and vice versa. Right: HOE with eight projectors.

4.2 Motion Parallax

Motion parallax is the apparent dynamic displacement of objects due to observer motion, and is a highly effective cue for spatial understanding, in particular when combined with stereoscopic displays [72, 73]. Motion parallax requires accurate and robust tracking of the observer's viewing position. Optical trackers such as OptiTrack [74] estimate the position and orientation of an object by illuminating with infra-red light a set of reflective markers attached to a tracked object. Head-tracking can be achieved by placing the

markers on the user's head, for example on a pair of stereoscopic glasses; see Figure 19. There are very few studies of systems that combine stereo, motion parallax, and haptics [75]. The surgery planning system described in Publications I and II and the surgical bone saw simulator described in Publication III provides the visualization cues surgeons use in real surgery: binocular vision and parallax from observer motion, while at the same time co-locates the visual and haptic workspaces.

Figure 19. Shutter glasses with reflective markers.

4.3 Visuo-Haptic Co-Location

In the physical world, our visual and haptic perception is co-located, that is, we can touch and *feel* an object in the same spatial location as we *see* it. This is so natural that we do not reflect upon it. In virtual environments however, such visuo-haptic co-localization cannot be taken for granted.

When a haptic device is used in combination with a visual display, they are often placed at some distance from each other; the graphical and haptic workspaces are non-collocated [76]. In such configurations, typically a graphical stylus, or avatar, within the graphical workspace mimics the motions of the haptic device. This type of indirect manipulation, similar to the mouse and pointer paradigm, is possible because the human brain is able to re-map some spatial offset between vision and touch [77].

By registering, or co-locating a haptic workspace with a visual workspace, the haptic and visual cues coincide and interaction with virtual objects becomes similar to what we are familiar with in the real world. Figure 20 shows a display rig from DevinSense AB [78] built specifically to accommodate such co-location. The user views the reflection of a stereo monitor mounted at an angle above a half-transparent mirror. Virtual 3D graphical objects visualized on the monitor appear to be suspended in the air below the mirror, where a haptic device may be placed such that the workspaces coin-

cide. The vantage point of the observer has to be known in order to accurately register the workspaces. Head-tracking enables a continuous update of the perspective of the 3D object according to the user's head motions. In Publication VII we evaluate how visuo-haptic co-location affects completion time and accuracy for interaction tasks in two visuo-haptic systems: one with a holographic optical element, and one with a half transparent mirror.

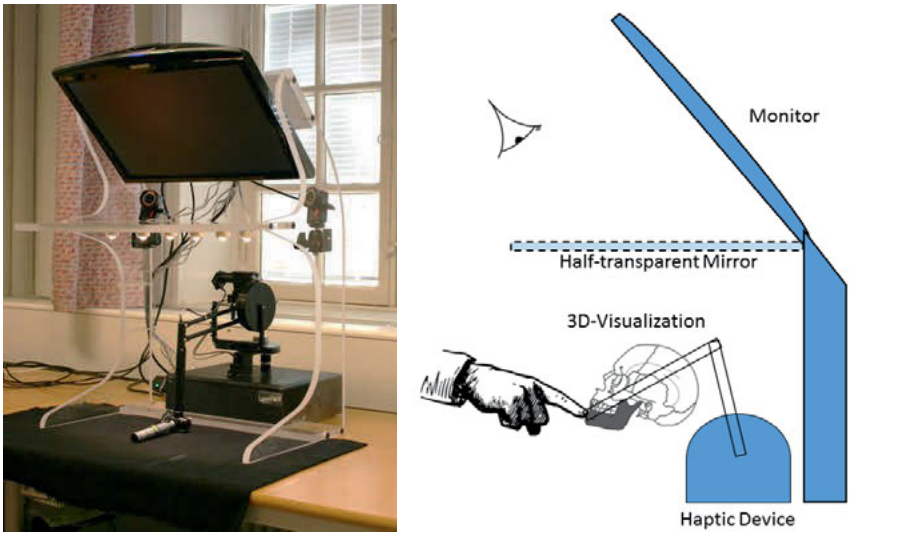

Figure 20. Left: Half-transparent mirror rig for visuo-haptic co-location with two tracking cameras mounted under the monitor. Right: Half-transparent mirror rig principle. A stereo monitor displays a 3D graphical model of a cranium, which is reflected on a half-transparent mirror such that it appears to be suspended in the air under the mirror. A haptic device under the mirror allows interaction with the 3D-model.

5. Cranio-Maxillofacial Surgery

Patients with tumors, trauma, or congenital defects in the head and neck region require cranio-maxillofacial (CMF) surgery. Approximately 560,000 cases of head and neck cancer are diagnosed annually worldwide, and about 300,000 patients die annually from these conditions [79]. Traffic accidents are a major cause of severe injuries with trauma to the face and head for 50-75% of the survivors [80]. Of 10,000 live births, four to five infants are born with severe deformities and another one or two with mandibular anomalies that require surgery [81]. CMF surgery to restore anatomy in patients with severe conditions from tumors, congenital defects, or trauma, such as gun-shot wounds, work related injuries, or traffic accidents, is both complex and time consuming. The outcome of the surgery affects both function and aesthetics and has a profound impact on the patient's quality of life. Aspects which affect the outcome include the skill of the surgeon, time from diagnosis to treatment [82], and quality of the preoperative plan [83, 84].

5.1 Virtual Surgery Planning

Virtual surgery planning (VSP) uses computer systems to visualize and enable interaction with virtual models of patient-specific anatomy, as part of a pre-operative planning process. Careful pre-operative planning leads to a better functional and aesthetic outcome, and at the same time leads to reduced time in the operating room [84-86] with considerable cost savings [87]. Vannier et al. demonstrated in a seminal publication from 1983 the use of 3D computer graphics to facilitate surgical planning in more than 200 clinical cases [88].

VSP allows a surgeon to inspect the anatomy of the individual patient prior to surgery and to virtually plan the surgical procedure. A plan could for example define how bone fragments ideally should be positioned in trauma cases, or how a mandible should be reconstructed with transplanted tissue in tumor cases. Planning may also involve the design of patient-specific fixation plates, cutting guides, and implants. Such planning also gives surgeons and engineers an opportunity to solve medical and technical patient-specific issues pre-operatively. Per-operatively this could also make the surgery less invasive, reducing the risk of soft tissue complications and morbidity.

Although the power of VSP systems have evolved dramatically since Vannier's first demonstration, commercial VSP systems of today, such as those from Brainlab [89] and Materialise [90], rely on the classical Windows, Icons, Menus, and Pointer (WIMP) paradigm; in essence 2D interfaces for interaction with 3D images of the human body. This has proved difficult for surgeons to use. Therefore, in clinical practice, the planning including the design and manufacturing of cutting guides, plates, and implants is often outsourced, relying on technicians or 3D-modeling experts to carry out complex designs; see Figure 21. This process often requires several iterations with the surgeons, causing a lead time to surgery of several days or even weeks. Time and cost would be reduced significantly if the surgeon could design implants without the help of a technician, and the required implants and plates could be produced in-house. This requires a user-friendly planning system that can easily be used by the surgeons themselves.

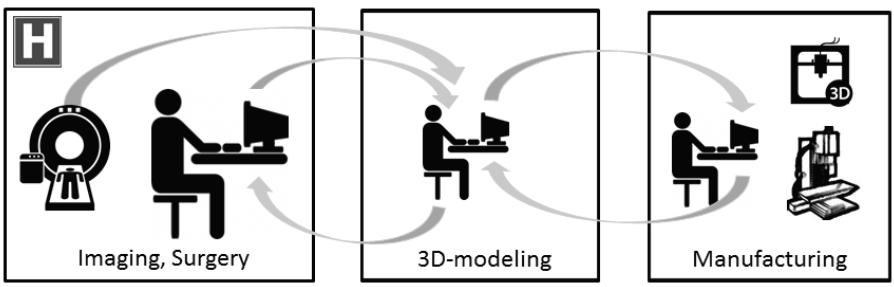

Figure 21. Outsourced surgery planning workflow. The hospital performs imaging and surgery locally, but outsources surgery planning, modeling, and manufacturing in a time-consuming iterative process.

5.1.1 Physical 3D Models

Conventional VSP systems offer the possibility of pre-operative planning, but their 2D interfaces makes it difficult to gain the necessary understanding of all spatial relations, especially for surgeons that are not used to working with computer assisted design software. Many surgeons order 3D printed patient-specific models to gain a better understanding of a case; see Figure 22. The surgeon may explore the models directly with his or her hands and view them from different angles. Physical models also play an important role in the search for optimal *occlusion* (contact between teeth) and they may also be used as a template to bend fixation plates pre-operatively. External production of such models however increases lead-time to surgery, and the image conversion and printing process may distort the resulting model [91].

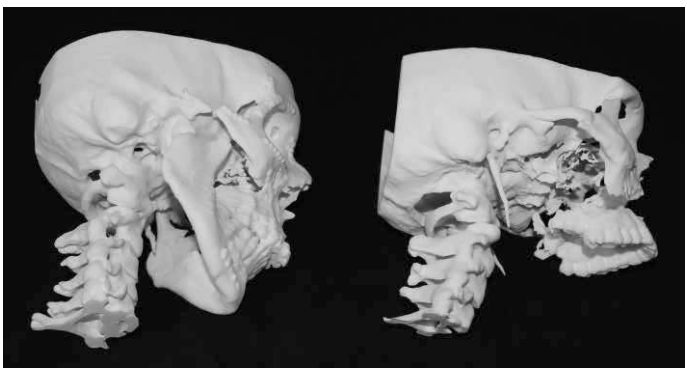

Figure 22. Anatomical patient-specific models produced with stereo-lithography.

5.1.2 Fracture Surface Alignment

Bone fragments in trauma cases may be displaced significantly, especially when the trauma is a result of high-energy impact. They may also be missing completely, as in some gun-shot cases. For the fractured bone to heal in a timely fashion and without deformity, the fragments must be re-aligned to their correct anatomical positions. In some cases, the fracture surfaces are complementary; see Figure 23, and in such cases they may provide a cue for alignment. The fragments “fit” together as pieces in a puzzle. This suggests the use of automatic, or semi-automatic, methods to assist in the surface matching and alignment process.

Figure 23. Mandibular bone fragments with complementary fracture surfaces. The fragments fit together as a puzzle.

Fully automatic virtual reconstruction of fractured objects have been suggested by several authors [92, 93], however the robustness of such methods is dependent on the quality and completeness of the data. The fracture surfaces may be more or less distinct depending on for example cause and age of the fracture, and proper placement generally requires anatomical knowledge, which motivates a semi-automatic approach.

One well-known example is the iterative closest point (ICP) algorithm for spatial alignment of two geometric point-clouds, denoted source and reference [94]. The user first places the source and reference in a coarse initial alignment. The algorithm then matches the closest reference point to each source point and estimates a rotation and translation using a mean squared error cost function that minimizes the mean offset between all matched points. The source points are transformed according to the previous step, and the algorithm iterates until the transformation magnitude falls below a predetermined threshold. Mellado et al. employ this method for semi-automatic reassembly of fractured archeological artifacts, however without collision detection or haptic feedback [95]. In Publication IV we describe a semi-automatic alignment tool that incorporates stable haptic feedback.

6. Contributions

This chapter briefly presents the methods and results described in detail in the appended publications. The previous chapters provide background and context to the work described herein.

6.1 The Haptics-Assisted Surgery Planning (HASP) System

The haptics-assisted surgery planning (HASP) system, developed within the scope of this thesis, combines haptic feedback with stereo visualization and motion parallax to allow a surgeon, with minimal system training and without support of technicians, to plan and test alternative solutions for complex trauma and oncology cases in less than one hour. Figure 24 shows the system hardware, and Figure 25 shows an overview of the workflow.

The HASP workflow starts with interactive semi-automatic segmentation of patient-specific CT images (and CT-angiograms in oncology cases) to separate bone structures from soft-tissue, to separate and label individual bones and bone fragments, and to segment relevant blood vessels. Several semi-automatic segmentation methods may apply; we use *BoneSplit*, developed by Nysjö et al. [64] for bone segmentation, and a semi-automatic method based on a tubular tracking algorithm described by Friman et al. [65] for blood vessel segmentation.

This thesis focuses on the subsequent use of the segmented data for analysis, planning, and testing of alternative surgical plans for complex trauma cases in Publication II, and for oncology cases with fibula osteocutaneous free flaps (FOFF) in Publication I.

HASP allows a surgeon, or a team or surgeons, to explore patient-specific anatomy preoperatively and freely touch, move, and rotate objects such as bone fragments, fibula segments, or vessels with the haptic device in a manner similar to manipulating real, physical objects. The surgeon may also use the haptic device to rotate the entire working volume or simply move his or her head to view the working volume from different angles, here referred to as “look-around”. Haptics may provide information that is difficult to perceive visually, for example the optimal fit between bone fragments in trauma cases.

Once a satisfactory plan is found, HASP may, in the future, support the design of tools to transfer the plan into the operating room including cutting guides and patient-specific fixation plates to be produced with additive manufacturing. Although these components are part of future work, they constitute an important element in the planning workflow, as in-house planning, design, and production of patient-specific devices enable considerable cost savings, and allow surgery on trauma patients within hours, rather than days that out-sourced planning and production require today.

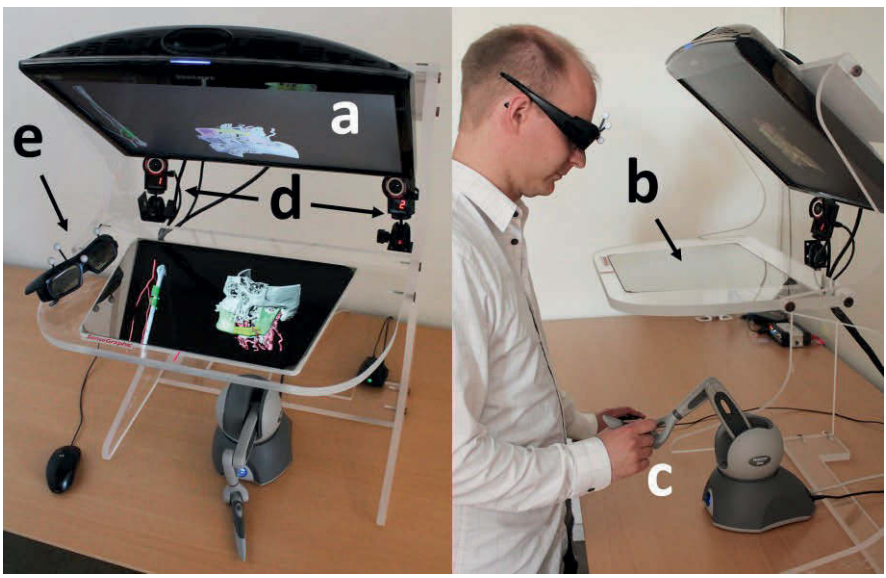

Figure 24. HASP hardware as seen from above (left) and from the side (right). A monitor (a) displays the anatomical 3D-model, which is reflected on a half-transparent mirror (b). A user manipulates a 3D-model with a haptic device (c) under the mirror. Two infra-red cameras (d) track reflective markers mounted on a pair of stereo glasses (e) for user look-around.

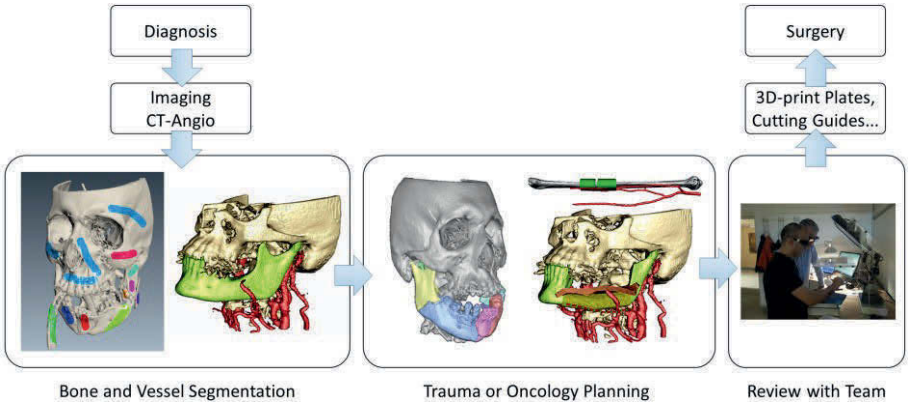

Figure 25. Overview of the HASP planning workflow.

6.1.1 Virtual Planning of Skeletal Reconstruction in Complex Trauma Cases

High-energy impact to the head and neck from for example car accidents or gun-shots often cause extensive trauma with complex fractures to the facial skeleton. Pre-operative planning is critical in cases such as the example shown in Figure 26 (left) where the patient fell from a sky-lift at a construction site, breaking the mandible (lower jaw) into more than ten fragments. Fracture surgery resembles solving a 3D puzzle with very high accuracy requirements. Even small offsets or angular errors in the positioning of each bone fragment may accumulate in the reconstruction of a series of fragments and result in poor function and a poor aesthetic result. Limited view during surgery, in combination with difficulty to maintain a complete understanding of the spatial relations between all bone fragments, makes adequate freehand reconstruction very difficult.

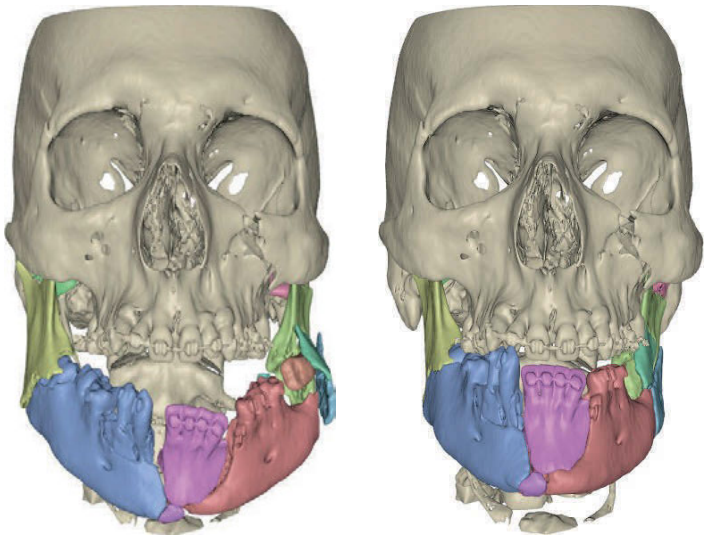

Figure 26. Left: Complex trauma case before virtual planning.[3] Right: Result after 22 minutes of planning in HASP.

In Publication II we describe how HASP can be used as a virtual, and more flexible, alternative to working with 3D-printed physical models to gain an understanding of complex trauma cases. When the user moves or rotates virtual bone fragments in the system, distributed contact forces and torque from contacts with other fragments give the user an impression similar to that of manipulating real, physical objects. We use a six-DOF quasi-static virtual coupling to maintain haptic stability. As penetration between fragments may be difficult to discern visually, haptic contact forces help the user to avoid improper placement of fragments during planning. When two or more fragments are positioned satisfactory, the user may group and manipulate them as one unit. Fragments may subsequently be added to or removed from the group.

6.1.1.1 Evaluation and Results

An experienced CMF surgeon from the Uppsala University hospital, who had never used HASP before, completed on his own the reconstruction shown in Figure 26 (right) in 22 minutes after 45 minutes of assisted training on a different case. The fractures in the mandible are adequately reduced (aligned). It was not possible to obtain perfect occlusion (contact between teeth) due to inference from dislocated teeth. The surgeon made extensive use of the grouping tool to build groups of fragments once he found a good

[3] Published with permission from the patient.

fit. He also used the head-tracking feature more and more throughout the session to look around objects instead of relying on object rotation to get good visibility. He noted that he could perceive haptically when a bone fragment under manipulation did not fit due to misplacement, or due to inadequate reconstruction of previously positioned fragments. He also commented that the system is useful for understanding the complexity of the specific case, and that he during the planning process gained insights on preferred order of fragment placement; assembling the fragments in a certain order may provide valuable clues towards the best global reconstruction.

6.1.2 Snap-to-fit

In Publication IV we describe *Snap-to-fit*, a semi-automatic alignment tool that assists a user in precise alignment of virtual bone fragments in trauma cases. We also test it on fractured archaeological artifacts.

6.1.2.1 Usage Example

Figure 27 illustrates an example of bone fragment alignment with Snap-to-fit. The user begins by marking the fracture surfaces with a tool that resembles a paintbrush, and then moves one of the fragments close to a potential matching fracture surface on another fragment. From this approximate initial position the user activates Snap-to-fit, which pulls the manipulated fragment toward the closest local stable fit, that is, it snaps the fragments into place. The user may influence the manipulated object's pose by pulling the object in different directions with the haptic interface. This allows a search of the neighborhood for the stable fit that the user deems best.

Figure 27. Snap-to-fit. Left: The user paints the fracture surfaces. Center: Initial, coarse fit for the bone fragments. Right: Aligned fragments.

6.1.2.2 Algorithm

To align two fragments, the tool computes an attraction force whose strength is proportional to an estimation of co-linearity between the local normals of the fracture surfaces. When two surfaces fit well together, their normals are approximately collinear; see Figure 28.

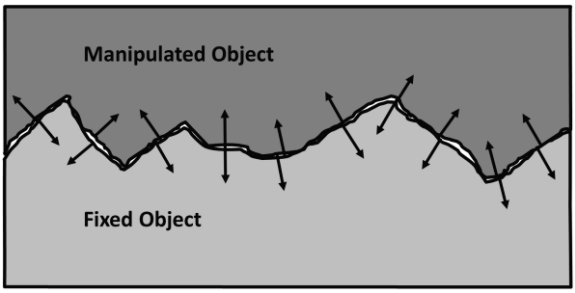

Figure 28. Matching surfaces with co-linear normals.

To test normal co-linearity, snap-to-fit employs an augmented Voxmap-Pointshell object representation, where the precomputed voxmap is defined not only inside the objects, but also in an *external* region outside the objects. In each voxel in the external voxmap, in addition to the closest distance to the object surface, the voxel also stores a local approximate voxmap gradient direction. The gradient direction approximates the surface normal direction on and close to the surface. Snap-to-fit computes attraction forces for the parts of the pointshell on the manipulated object that are closer than a predefined threshold distance to the fixed object. A pointshell point's distance to the fixed object can quickly be found by retrieving the fixed object's external voxmap value at the point's position. For each included pointshell point, the scalar product between the surface normal at the pointshell point and the gradient direction of the fixed object's external distance map at the same point serves as a matching metric for that particular pointshell point.

Snap-to-fit combines the attraction forces with distributed contact forces that prevent fragment penetration, and a quasi-static six-DOF virtual coupling for stability; see Figure 29. These three sets of forces can be given different weights depending on the application; stiffening the virtual coupling gives a higher degree of control to the user. The attraction forces, the contact forces, and the virtual coupling also yield a torque around the grasp point. In a manner similar to conventional quasi-static virtual coupling, the manipulated fragment assumes a position and orientation where all forces and torques are in equilibrium.

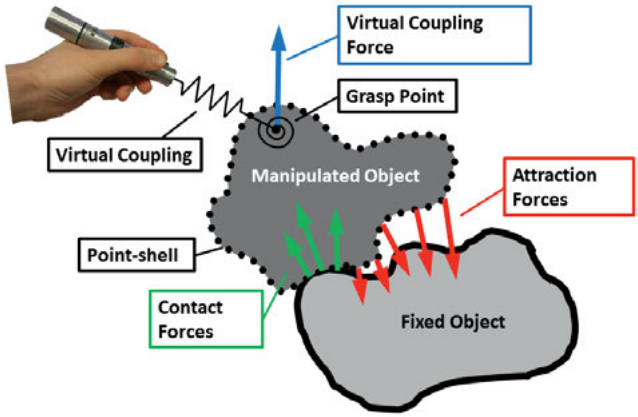

Figure 29. Three sets of forces and torques act on the manipulated object: six-DOF virtual coupling, contact force/torque, and attraction force/torque.

Snap-to-fit works best when the fracture surfaces are complementary, well-defined by the segmentation, and not too small. If the fracture surfaces are damaged, for example in compression fractures or gunshot injuries, snap-to-fit may not find a good match between the fracture surfaces and the user has to use his/her expertise to manually find a suitable placement.

6.1.2.3 Evaluation and Results

In Publication IV we test snap-to-fit in one trauma case and one archaeological case and achieve stable fits at a sampling rate of 1 kHz for surfaces with over 5000 points.

6.1.3 Virtual Planning of Bone, Soft-tissue, and Vessels in Oncology Cases

Mandibular tumor cases often require transplantation of bone, vessels, and soft tissue to reconstruct the anatomy after tumor removal. Todays most established reconstruction procedure is the *fibula osteocutaneous free flap* (FOFF), first described by Hidalgo in 1989 [96]. It is based on the grafting of a part of the fibula (calf bone), along with supplying vessels and often a part of the skin (skin paddle) to cover soft tissue deficits [97]. The surgeon cuts the fibula into one or multiple segments shaped to recreate the original mandibular contour, and connects the transplanted vessels to vessels in the head/neck to maintain vascularization of the transplant; see Figure 30. Such procedures require a high degree of surgical skill, and have a long learning curve, especially in medical centers with a low case load.

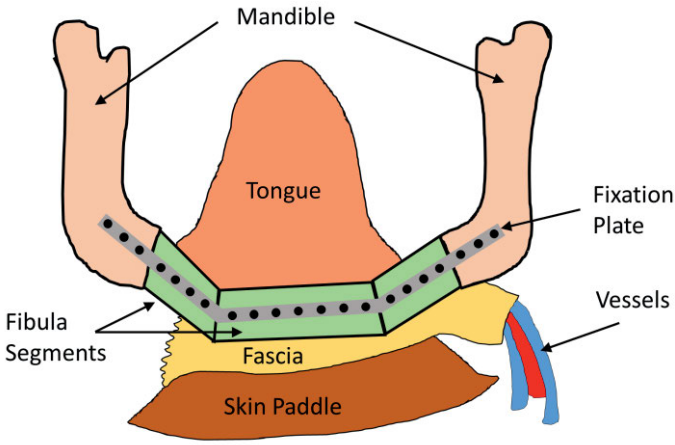

Figure 30. Mandibular reconstruction with a FOFF. After tumor removal, the fibula segments are cut such that they recreate the initial mandibular contour. The plate fixates the segments and keeps the reconstruction together.

In Publication I we describe how HASP supports preoperative planning of reconstructions with a FOFF in oncology cases. After segmentation; see Figure 31 (a), the surgeon begins the virtual planning by defining with a resection tool a region for removal that contains the tumor and a safety margin; see Figure 31 (b). The surgeon then defines the exact osteotomy (bone cut) positions and angles through the fibula required to restore the contour of for example a mandible; see Figure 31 (c). Distributed contact forces and torque from contacts between fibula segments and other bone structures give the user an impression similar to that of manipulating real, physical objects.

Several parameters must be considered in addition to finding the optimal contour. The orientation of the fibula segments must take into account future dental implants, osteotomies must not interfere with vessels that vascularize the transplanted fibula, and the transplanted vessels must reach potential anastomosis (connection) sites in the head/neck. If segmented CT-angiogram images from a patient's head/neck region and leg are available, HASP, in contrast to conventional planning software, provides a deformable model of patient-specific vessels in the leg, which allows interactive reachability testing to evaluate potential anastomosis sites; see Figure 31 (d). The virtual vessels provide a haptic cue similar to a rubber band if they are stretched. Finally, if transplanted skin is used to cover soft-tissue deficits, the configuration of the skin and the vessels that vascularize the skin must be considered. HASP provides a deformable model of a generic skin-paddle; see Figure 31 (e). An interesting direction for future work would be to incorporate

patient-specific deformable skin. HASP allows a surgeon to search for an optimal reconstruction both *interactively* and *iteratively* as illustrated by the middle portion of Figure 31.

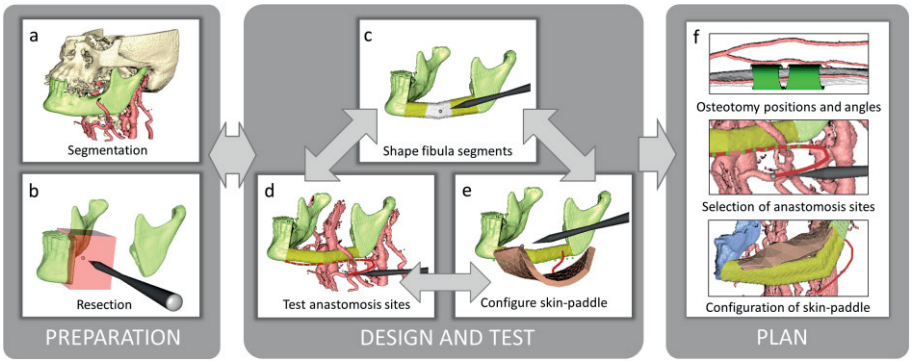

Figure 31. Iterative planning workflow. Left: preparation stage with segmentation (a) followed by resection (b). Center: Iterative design of fibula segments (c), test of anastomosis sites (d), and configuration of skin-paddle (e). Right: Resulting plan (f).

Figure 31 (f) illustrates the resulting plan, which comprises positions and angles for osteotomies in the fibula required to restore a desired contour. These metrics could be used to produce patient-specific cutting guides to be used during the actual surgery. The plan also comprises one or multiple potential anastomosis sites, and a configuration of a skin-paddle to cover soft-tissue deficits.

6.1.3.1 Evaluation and Results

One CMF surgeon and one plastic surgeon from the Uppsala University Hospital evaluated HASP with four retrospective oncology cases that they had previously operated on after conventional virtual planning. The first case served as practice; the surgeons received 40 minutes of instructions on how to use the system during the planning. After the practice, the surgeons could make a detailed plan of the subsequent cases in between 29 and 63 minutes per case.

Figure 32 shows the results of the planning of the four cases, presented in detail in Publication I. In some cases, problems during surgery could most likely have been avoided as they became evident during the planning with HASP. In Case 3, the fibula had to be rotated 180 degrees about its length axis intraoperatively to avoid plate and screw interference with a vessel. In Case 4, the fibula had to be reversed 180 degrees from the surgical plan de-

rived with conventional planning software, as the vessels did not reach the initially suggested anastomosis site. As a result, the distance between the bone and the fixation plate increased, the fit between the fibula segments became suboptimal, and the fibula did not reach the temporal fossa. In Case 2, it was difficult to find the optimal fibula shape and position resulting in extra time in the operating room. The surgeons estimate that the ischemia time (the time a tissue, organ, or body part has its blood supply disconnected during transplantation until it is reconnected to a blood supply) could have been reduced up to 25% in this case.

The surgeons appreciated the possibility to iterate between the different components of the FOFF (skin, bone, and vessels) during collaborative planning. The bone defect was easily visualized, and the surgeons could adjust where on the fibula to place the osteotomies to optimize the locations of the vessels to the skin paddle and the reach of vessels to potential anastomosis sites.

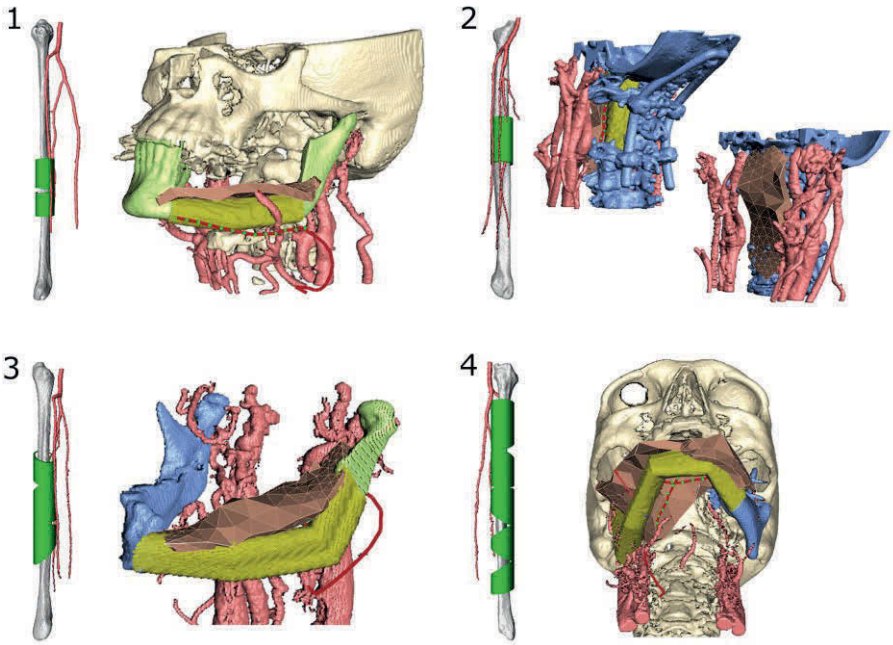

Figure 32. Final plans.[4] Case 1: osteoradionecrosis. Case 2: cervical spine defect. Case 3: ameloblastoma. Case 4: squamous cell carcinoma. To the left in each case the whole fibula with osteotomy positions and orientations is shown in relation to surrounding vessels.

[4] Published with permission from the patients.

Other feedback includes that the ability to work in 3D with "look-around" is very helpful for perception of the anatomy and alignment of objects. Haptic feedback assists the contouring of the reconstruction and the insetting of the FOFF, giving a striking difference to other systems without haptic feedback previously tried by the two participating surgeons. The haptic feedback was especially appreciated for the feel of the bone (resistance when hitting the ends of the resection) and when planning the length of the fibula.

The main areas for improvements concerned system ergonomics, including limited screen size, arm fatigue after extended use of the haptics device, and that only one user at a time can fully benefit from the head tracking.

6.2 Combining Kinesthetic and Vibrotactile Feedback in Surgery Simulation

Realistic haptic feedback in a simulator for training surgical bone sawing should reproduce the feel of a reciprocating surgical saw with its vibrations as the saw blade runs in free air or saws through bone. In addition to learning the appropriate levels of force to be applied to the saw handle, it is important to become comfortable with the vigorous vibrations from the saw while steadily creating an osteotomy into bone of varying thickness and density.

Several authors acknowledge the importance of vibrations in surgical tool simulation, but use unmodified commercial kinesthetic devices to display tool forces [98, 99]. Although kinesthetic haptic devices could to some extent produce vibrotactile feedback, such devices typically mediate force from their actuators to the user through a mechanical linkage with inherent dynamic properties such as inertia, friction, and sometimes backlash. Such linkage distorts vibrations and lowers the fidelity. In addition, sustained display of vibrations may cause undue wear of the device, and the upper vibration frequency is limited by half the sampling rate according to the Nyquist theorem [100].

6.2.1 Hybrid Haptic Actuation

In Publication III we describe how hybrid actuation can increase realism for a surgical saw simulator. In our simulator, a vibrotactile actuator, a Haptuator from Tactile Labs Inc. [101], placed in proximity to the user's hand, superimposes high-frequency vibrations over low-frequency kinesthetic feedback from an off-the-shelf commercial device; see Figure 33. The vibrotactile actuator reproduces high-frequency vibrations which are prerecorded

with a contact microphone from an actual reciprocating surgical saw, while running it in free air, and while cutting bone at various reciprocating rates; see Figure 34.

Figure 33. A vibrotactile actuator (lower right) embedded in a handle that resembles a real surgical reciprocating saw, reproduces vibrations previously recorded from an actual surgical saw.

Figure 34. Contact microphone attached to a reciprocating surgical saw.

6.2.2 Kinesthetic Haptic Rendering

A contact force simulation computes kinesthetic haptic feedback at a rate of 1 kHz by uniform sampling of 132 points distributed in three rows on a virtual saw blade, and determines force directions and magnitudes from the corresponding positions in a precomputed distance map within the bone model, where the voxel values correspond to the voxel distance from the model surface. The contact forces are given the direction of the negative distance map gradients and are scaled by distance map values in the model,

which yields repelling forces with magnitudes proportional to the blade penetration depth.

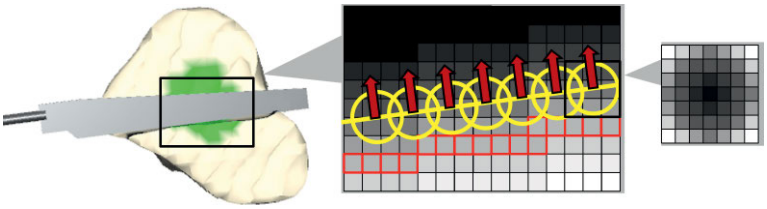

Figure 35. Virtual saw blade sawing though bone (left). Cutting kernels (yellow circles and magnification to the right), contact forces (red arrows), visualized iso-surface (red squares).

Each sample point on the blade provides haptic contact force, and we remove bone material around the saw blade teeth at a graphical rate of approximately 60 Hz by decreasing the voxel values using precomputed radial-basis-function kernels to retain the gradient at the bone boundaries; see Figure 35. The removal rate is inversely proportional to the bone density. At a predefined distance map value we derive an iso-surface for model surface visualization. Human bone has heterogeneous density, with maximum density in the cortical (outer layers) of the bone, and decreasing density towards the inner cancellous bone. Therefore, the model also contains a density map derived from Hounsfield values in the CT data, in which increasing density corresponds to increasing Hounsfield values. Differences in density are mapped to colors in the bone visualization; as an example, the dense cortical bone is white and the less dense core is green, as seen in Figure 35.

6.2.3 Evaluation and Results

To analyze how accurately the vibrotactile actuator reproduces reciprocating saw vibrations, we run prerecorded vibration sequences in the simulator while recording the vibrations from the simulator handle with the same contact microphone previously used to record the actual surgical saw. Figure 36 shows frequency spectra of authentic vibrations from the actual saw, denoted by *saw*, and vibrations from the simulator handle, denoted by *sim*.

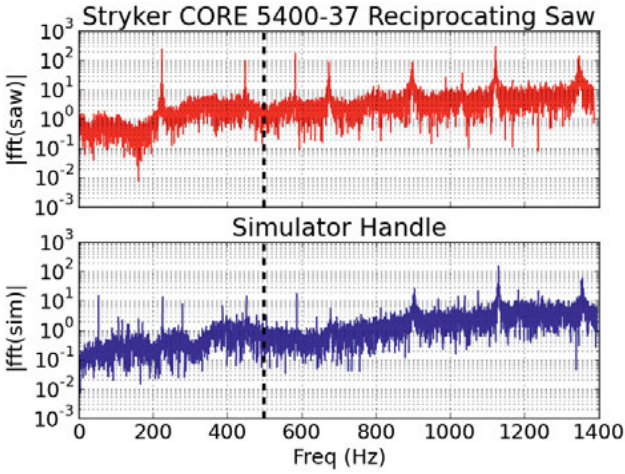

Figure 36. Frequency spectra from the real saw (above) and the simulator handle (below). The virtual bars indicate the approximate limit for human vibrotactile sensing, 500 Hz.

We observe that the overall shapes of the two spectra are very similar, also well above the limit of human sensing, and the spectral peaks in saw also appear in sim. Differences in the spectra can be attributed to differences in the material properties in the two handles, and the fact that the vibrotactile actuator is unable to generate the same power as a real reciprocating saw. The 50 Hz peak in sim is most likely due to insufficient filtering of the power supply to the Haptuator amplifier. The 233 Hz peak in the saw spectrum corresponds to the maximum reciprocation rate of the saw, and higher frequency peaks are likely to be from higher order harmonics, and saw teeth interaction with bone.

6.3 Haptic Grippers

In body-grounded haptic grippers the actuator bulkiness and weight is more critical than for grounded devices such as the Phantom devices where the user does not carry the weight of the actuators.

Piezoelectric motors, in contrast to EM motors, offer higher force-to-volume ratio at the motor shaft (without gearbox) [102], a desirable property for integration into haptic grippers. Their operational velocity is generally much lower than EM motors, and their maximum continuous force/torque is higher, which allows direct-drive without reduction gearing and backlash.

In Publications V and VI we describe the design and evaluation of two haptic grippers actuated by piezoelectric motors of different types: a walking quasi-static motor (WQSM) and a traveling-wave ultrasonic motor (TWUM); see Figure 37 and Figure 38, respectively.

6.3.1 Gripper Actuated by a Walking Quasi-Static Motor

In Publication VI we present a one DOF gripper actuated by a Piezo LEGS® LT2010 WQSM from PiezoMotor AB [38]; see Figure 37 (A). The DOF is the rotation of the metacarpophalangeal (MP) joint (B) of the index finger for a precision grip between the thumb and index finger. The user places his/her thumb in the tube (C) and the index finger in the thimble (D). To account for varying hand sizes, the thumb tube can be lowered or raised by releasing the screw (E). The index finger part (F) moves along an arc with its rotational axis close to the MP joint. To constrain the motion of the index finger part to the desired arc, we use a curved rail, guided relative to the mainframe of the gripper by four ball bearings on each side of the finger part. The WQSM drive rod drives the index finger part via a rotational joint consisting of a 1 mm diameter steel pin that uses the plastic material of the index finger part as bushing. The selected leverage magnifies the motor speed about four-and-a-half times at the index finger thimble (resulting in a maximum speed of 70 mm/s with an index finger part length of 70 mm), while the maximum force is reduced with the same factor.

This design with a linear motor and a curved guide makes it possible to add additional DOF's in parallel for the remaining fingers. A magnetic position encoder (G) from Nanos Instruments with a resolution of 16,000 pulses/mm detects the movements of a magnetic rod (H) attached to the piezoelectric motor's drive rod (I), which is mostly hidden by the mainframe in the image. A strain gauge sensor (J) from Tokyo Measuring Instruments Laboratory (TML), mounted in a full bridge arrangement on the index finger part,

measures forces applied to the thimble in the positive and negative directions orthogonal to the index finger part. We calibrate the strain gauge sensor by repeatedly applying known force levels orthogonally to the finger thimble with a Newton meter to confirm linearity, and estimate the force constant by linear regression. Most parts are printed using stereolithography and the gripper attaches to a six-DOF Phantom arm [17] with the connector (K) resulting in a seven-DOF system. A PMD90 module from PiezoMotor generates the amplified motor signal, and samples the signals from the strain gauge sensor and the position encoder.

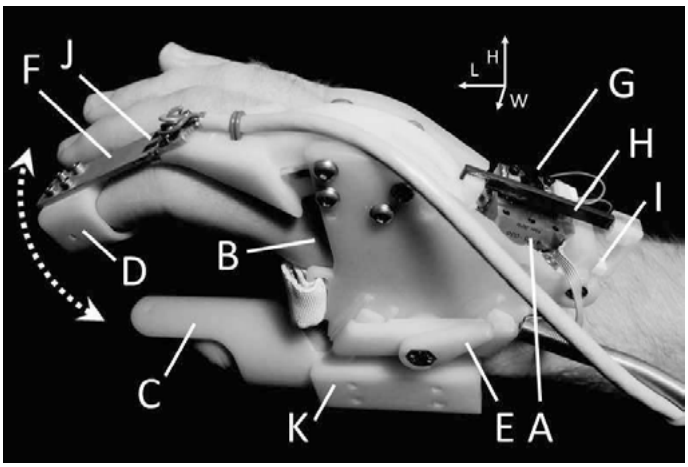

Figure 37. Gripper actuated by a linear WQSM: Piezo LEGS® LT2010 (A); rotational point (B); thumb tube (C); index finger thimble (D); size adjustment screw (E); index finger part (F); magnetic position encoder (G); magnetic rod (H); motor drive rod (I); strain gauge sensor (J); connector for Phantom device (K). The dashed arrow indicates finger part motions.

6.3.2 Gripper Actuated by Traveling-Wave Ultrasonic Motors

In Publication V we present a comparison between the WQSM gripper described above, and a gripper with two DOFs, actuated by two rotational PUMR40E TWUMs from Piezotech [103]; see Figure 38 (A, B). The DOFs are first a rotation close to the metacarpophalangeal (MP) joints of the index, middle, and ring fingers, for a precision grip against the thumb, and second a rotation close to the carpometacarpal (CMC) joint of the thumb around an axis that permits opposition (contact) and sliding against the remaining fingers. These two DOFs enable operations such as fastening a virtual screw or balancing a virtual object between the fingers. The user places his or her

thumb in the thumb thimble (C), and the index, middle, and ring fingers on the finger plate (D). Straps hold the fingers in place (E). The two TWUM's are mounted such that the rotational axes of the motors (indicated by dashed lines) are closely aligned with the axes of the finger joints. The parts in contact with the user's fingers are rigidly attached to the motor axes, without gearing. This direct-drive configuration assures backlash-free operation.

Optical angular encoders with a resolution of 4000 pulses/revolution integrated into the motor housing measure the angular positions of the finger thimble and plate. Custom strain gauge torque sensors mounted in series with the motor shafts measure user forces (F). We calibrate the torque sensors in the same manner as for the WQSM gripper. The gripper attaches to a six-DOF Phantom arm with the connector (G) resulting in an eight-DOF system. We generate motor signals for the TWUM with a WGM-201 signal generator from Syscomp Electronic Design, and amplify the signals with a PMC1200 module from PiezoTech. The PCM1200 on-board signal generation is insufficient for haptic applications due to its high latency. An Arduino Uno board handles the angular encoder signals, and a DSCUSB-board from Mantracourt handles the strain gauge signals.

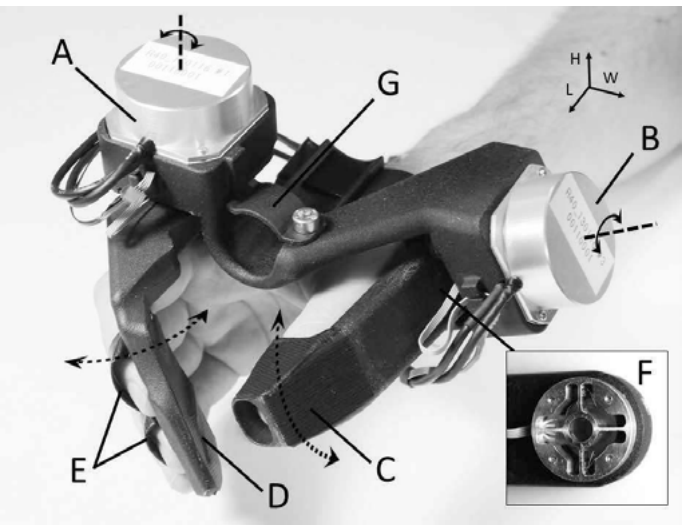

Figure 38. Gripper actuated by two rotational TWUMs: PUMR40E (A, B); thumb thimble (C); finger plate (D); finger straps (E); torque sensor (F); connector for Phantom device (G). Dashed arrows indicate finger part motions.

6.3.3 System Architecture and Control

Figure 39 shows a system schematic that applies to both grippers, although the details of the individual components differ. It is based on a classical admittance control scheme with an inner control loop, commonly employed in robotics [104]. A human operator applies a force F_h to the device, sampled by a force sensor. The sampled force F_s drives a virtual object model. In Publication V, this model simulates a spring and a damper mounted in parallel, parametrized by a stiffness of k N/mm and a damping of b Ns/mm, respectively. The dynamic behavior of the model can be described as a first order differential equation relating position, velocity, and applied force: $kx_d(t) + b\dot{x_d}(t) = F_s(t)$. Although omitted in our experiments, a second order inertial term could be added. In Publication VI, the model consists of a set of look-up tables relating applied input forces to output deflections, derived from measurements on physical elastic objects. The positional state of the model, x_d, serves as a desired position, and an inner control loop (within the dashed box) drives the motor towards x_d. The inner loop is a positional controller with a gain K that is set as high as possible without losing stability in order to minimize the error, x_e, between the desired position/angle, x_d, and the sampled position or angle, x_s. The scaled error serves as a drive command, V_c, to a motor-specific driver. Depending on V_c and driver mode parameters, the motor sets the gripper interface mechanics into motion, x_o, that is fed back to the human operator. An encoder samples the motor position, and the sampled position x_s is fed back to the inner position loop. The system runs at a fixed rate of 150 Hz.

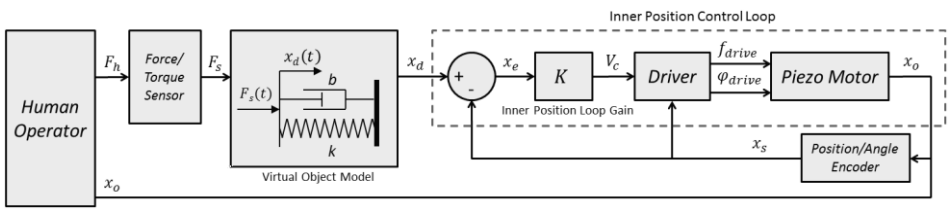

Figure 39. Gripper schematics. The grippers differ in force sensors, position encoders, drivers, and motors.

6.3.4 Evaluation

One important objective when designing haptic interfaces is that they reproduce the *feel* of interacting with a physical object. A quantitative method to evaluate this is to analyze how the interface responds to applied

forces, and how well the response matches the response of a simulated virtual object with known properties. We call this admittance fidelity. One could argue that the perception of an object is much richer than simply its response to applied forces. Indeed, in order to fully realize Sutherland's vision of the ultimate display, a haptic gripper should be able to display temperature, heat transfer, and fine surface features. In Publication V however, we constrain ourselves to test admittance fidelity by exposing the two grippers to repeated sinusoidal forces using a test rig while simulating and displaying simple virtual objects; springs of various stiffness, dampers, and rigid walls, common basic building blocks in more complex virtual environments.

6.3.4.1 Test Rig

For systematic testing of the haptic grippers, we constructed a test rig that generates sinusoidal oscillating forces and motions at various rates; see Figure 40. A servo motor (A) with adjustable speed drives a loop of non-elastic cord (B), led over two rotational pulleys (C), in a sinusoidal oscillation with a peak-to-peak amplitude of 50 mm. Two extension springs (D) mounted in series with the non-elastic cord establish a pre-load tension in the cord. A point (E) on the cord, between the springs, connects to a finger part of a gripper (F). The gripper is oriented such that the cord exerts approximately orthogonal forces to the finger part. We chose a spring constant of 0.19 N/mm, yielding an effective stiffness of 0.38 N/mm at the connection point, owing to the antagonistic configuration of the two springs. During an oscillation cycle, the peak cord velocity is limited by the oscillation rate of the cord and the resistance by the haptic device. For example, at 1 Hz, the peak zero-load rig velocity is $50\,\mathrm{mm} \cdot \pi \cdot 1\,\mathrm{Hz} \approx 157\,\mathrm{mm/s}$.

If a gripper displays free motion, the oscillating cord constitutes a position source following a sinusoidal trajectory: the extension springs maintain force equilibrium with a net force close to zero at the connection point. However, if the gripper displays a rigid wall, the cord becomes a sinusoidal force source. Here, the extension springs become unequally stretched, building a net force at the connection point until the holding force of the piezoelectric motor is exceeded, or the cord changes direction. Thus, depending on the haptic simulation, the test rig acts as an oscillating position source, a force source, or a combination of the two.

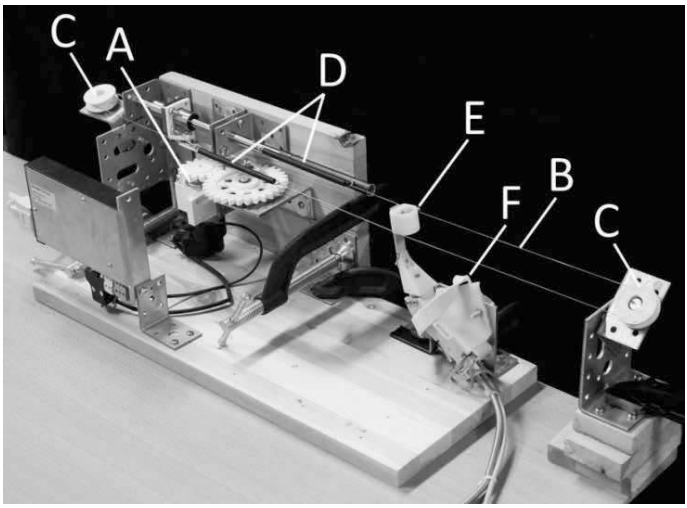

Figure 40. Admittance fidelity test rig: A servo motor (A) drives a cord (B), that is led over two pulleys (C) and pre-loaded by extension springs (D), in a sinusoidal oscillatory motion. A point (E) on the cord connects to a finger part of a haptic gripper under evaluation (F).

6.3.5 Results

The evaluation and comparison between the grippers described in detail in Publication V shows that the WQSM is superior to the TWUM as an actuator for applications where accurate tracking and very stiff feedback at low velocities is desired, such as in fine manipulation tasks. The lowest velocity of the WQSM depends only on the driving electronics, and its velocity and position are very straightforward to control also at very low velocities. The WQSM also provides higher force than the TWUM, and is smaller and lighter. However, the WQSM needs leverage to reach desired maximum velocities in our gripper, which requires careful design, and its limited maximum velocity severely limits its performance at higher velocities. In addition, the WQSM operates at audible frequencies which is disturbing if an application requires silent operation. For applications where high velocity is required, for example in game controllers, a TWUM is a better option. TWUMs also provide a “low friction” mode for the display of free motion, and can, depending on drive mode, operate inaudibly.

6.4 Visuo-Haptic Co-Location

Stereo visualization in combination with head-tracking allows precise registration (co-location) between the visual and haptic workspaces in a visuo-haptic display. In Publication VII we evaluate the effect of such co-location on accuracy and completion time for interaction tasks in a visuo-haptic environment.

6.4.1 Experiment

We designed a user-study comprising three interaction tasks, of which two focused on spatial accuracy and one focused on completion time; see Figure 41. We hypothesized that co-location would improve both accuracy and completion time. Sixteen test subjects performed all three tasks in a co-located setting, where the haptic and visual workspaces were carefully spatially registered, and in a non-collocated setting where the workspaces were spatially offset by 30 cm. All tasks, both co-located and non-collocated were performed on two different displays described in the background section of this thesis; a half-transparent mirror display and a holographic optical element (HOE). To reduce learning bias, we divided the subjects into two groups, with one half starting on the HOE display and the other half on the mirror display. Both these groups were in turn divided into halves, with one half starting in the co-located mode and the other half in the non-collocated mode. Half of the subjects starting co-located on one display also began co-located tests on the other display, while the other half reversed the order when moving to the other display.

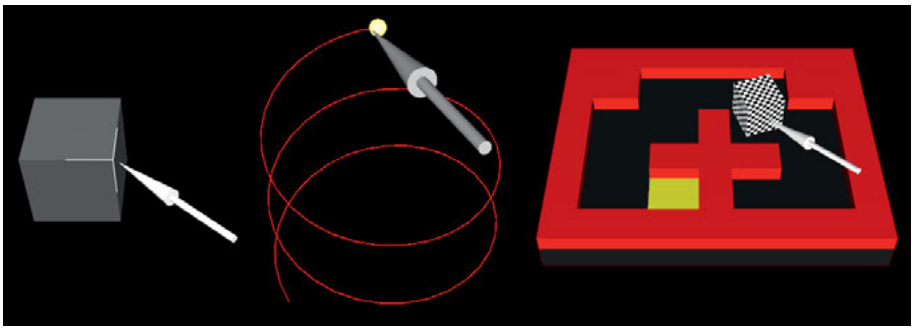

Figure 41. Interaction tasks. Left: accuracy task number one, point at the corners on a cube. Center: accuracy task number two, track a sphere along a spiral path. Right: manipulation task, push a cube through a labyrinth.

In the cube task shown in Figure 41 (left), we instruct the subjects to point as accurately as possible at the corners of a cube in a sequence indicated by a visual high-light. The performance metric is the average Euclidean distances between a user controlled pointer and the target corner positions.

In the spiral task shown in Figure 41 (center), we instruct the subjects to follow as accurately as possible a sphere that moves along a spiral path. Here, the average Euclidean distances between the user controlled pointer and the moving target sphere position serves as performance metric.

In the labyrinth task shown in Figure 41 (right), we instruct the subjects to push the black and white cube back and forth five times through a labyrinth. Here, the completion time serves as performance metric.

6.4.2 Results

This study, presented in detail in Publication VII, shows that co-location significantly improves completion time for the manipulation task on both displays. However, the study shows that co-location does not improve the accuracy in the spatial accuracy tasks.

7. Conclusions

In this section, we summarize the contributions of this thesis and suggest directions for future work.

7.1 Summary of Contributions

In the scope of this thesis, we have developed a prototype visuo-haptic system (HASP) for virtual surgery planning. We address two main applications; trauma reconstruction and oncology planning with composite transplants of bone, vessels, and soft-tissue, that is fibula osteocutaneous fibula flaps. We evaluate the system by letting surgeons, on their own, after a short training session, plan one retrospective trauma case, and four retrospective oncology cases. The potential of HASP reaches far beyond what is presented in this thesis, and will hopefully serve as a test-bed and development platform for future research.

For surgery training, we describe a surgical bone saw simulator with a novel hybrid haptic interface that combines kinesthetic contact forces between a virtual saw blade and a virtual bone model, with realistic vibrotactile feedback that is prerecorded from an actual surgical saw.

For semi-automatic alignment of fractured virtual objects, we present a stable attraction force model, *snap-to-fit*, suited for integration with established six-DOF contact rendering and quasi-static virtual coupling methods.

We evaluate how visuo-haptic co-location affects completion time and accuracy for interaction tasks in two visuo-haptic systems: one with a holographic optical element, and one with a half transparent mirror. We find that for our tasks in which accuracy, not time is the objective, co-location does not improve accuracy. However, co-location significantly improves completion time for our manipulation task in which completion time is the objective.

Finally, we design and evaluate two haptic grippers actuated by two different types of piezoelectric motors: a walking quasi-static motor, and a traveling-wave ultrasonic motor. We show that the walking motor is ideal for high-precision haptic tasks where the maximum velocity is low. When higher velocity is required, the traveling-wave motor is a better option.

7.2 Future Work

One important part of future work is evaluation. Although we have tested HASP on several clinical cases, they were all retrospective cases where the operations had already taken place. A large prospective study, ideally conducted at several hospitals, is needed to reach a satisfactory validation of the system. This study should also evaluate the value of the individual components of the system; haptics, stereo visualization, and parallax.

Another crucial part of future work is transferring the plan from HASP into the operating room. This includes tools for designing cutting guides and fixation plates for in-house production with, for example, 3D printers, but also the generation of a report with relevant measurements and screen captures from the plan.

It would be very beneficial to integrate interaction with deformable models of patient-specific soft-tissue into HASP, using for example SOFA [18].

The main purpose of the bone saw simulator proposed in this thesis is to demonstrate the combination of kinesthetic and vibrotactile feedback. Although the vibrotactile component of the simulator is very realistic, the kinesthetic component could be developed further for a higher level of realism.

We have shown that snap-to-fit is a stable six-DOF attraction model that can assist in the alignment of fractured virtual objects. However, the efficacy of the method should be further evaluated on a large set of fractured objects from various domains, for example bone fragments or archaeological artefacts. It may be fruitful to incorporate not only fracture surfaces in the alignment process, but also surfaces adjacent to the fracture and exploit that the outer contour of bones is often smooth and continuous across a fracture when the fragments are well aligned. It would also be interesting to augment snap-to-fit with global surface matching that searches for potential matching surfaces in the whole scene.

Two important issues with the gripper with the walking quasi-static motor are audible noise and speed. The motor used in the glove prototypes is a standard component for high precision movements and the maximum speed

does not allow very fast finger movements. An integrated clutch function could potentially be implemented by controlling the pre-load force of the stator against the drive rod, for example by a piezoelectrically actuated additional degree of freedom. By releasing the clutch, the drive rod can be moved freely. By adjusting the pre-load, a range of friction coefficients could be displayed, and when full force is applied, the system switches to admittance control. One challenge would be to ensure that the piezo-legs are not damaged when the pre-load is altered.

8. Acknowledgements

Although I know that I am unable to list them all, I would like to express my special appreciation to the following extraordinarily helpful and inspiring persons who contributed directly or indirectly to this thesis:

My main supervisor Ingrid Carlbom for believing in me, for sharing your expertise and experience, and for making me understand that anything is possible. (And for trying to teach me to say no sometimes...) I would also like to thank your wonderful family, Tom and Sarah, for your hospitality during my stays in New Jersey, it was truly a great experience! I look forward to seeing you again in Sweden or in the US.

My assistant supervisor Stefan Johansson, for always being positive and constructive, and for interesting conversations spanning the full spectrum between traveling, fishing, piezoelectric motors, and engineering in general.

My assistant supervisor Ewert Bengtsson for support, good advice, and for always showing great interest and encouraging my work.

The division head Ingela Nyström for running Vi2 with enthusiasm and care.

Fredrik Nysjö for showing such generosity and patience sharing your passion and knowledge of programming and computer graphics. It has been a pleasure working and traveling with you. I look forward to continuing our collaboration. Good luck with your Ph.D. studies!

Johan Nysjö, Hans Frimmel, Anders Hast, and Gustaf Kylberg, for being such wonderful companions in teaching the computer graphics course. It's been a great experience, and a lot of fun.

Stefan Seipel for fruitful collaboration on Publication VII and *SplineGrip*.

Anders Jansson and Mats Lind for your invaluable advice on user studies.

Lena Nordström for always being helpful, for reminding me about practical matters, and for sharing your passion for Australia.

Bettina Selig and Martin Ericsson, you made me feel like home day one.

Christophe Avenel for being such a humble and friendly genius.

Milan Gavrilovic for inspiring conversations about film and life in general, and for being an advocate of alternative working hours.

Elisabeth Linnér and Hamid Sarve for being you, for all the fun we had, for all the support, and for all priceless conversations in the “pancake club”!

Mikael Laaksoharju for interesting conversations about human-computer interaction, human-human interaction, music, and life in general.

Filip Malmberg for sharing your passion for science and music.

All other past and present colleagues and friends at Vi2. Thanks for being who you are, for great lunch conversations, and for making Vi2 such a friendly place!

Our collaborators at the Uppsala University hospital, Jan-Michaél Hirsch, Andreas Thor, and Andrés Rodríguez-Lorenzo, for introducing me to your exciting world, and for taking time to really explain, and show, how surgical procedures are done.

Daniel Buchbinder at the Mount Sinai Beth Israel Hospital, NYC, for your enthusiasm, for your support, and for your hospitality during my visit.

Neeru Singh at the Mount Sinai Beth Israel Hospital, NYC, for positive and constructive collaboration when writing Publication III.

Our artistic collaborators Björn Anéer, Hans Frimmel, and Esther Ericsson, for being open minded and bridging the gap between science and art.

Craig Carignan at UMD and Igo Krebs at MIT for opening my eyes (and my sense of touch) to the fascinating word of haptics and robotics, and for convincing me to go back to school.

Professor Heung-Kook Choi at Inje University, Gimhae, Korea, thank you so much for the hospitality you showed me during my visit.

Tony Barrera, for reminding me that in the galactic scope of things, our earthly hardships are indeed very small.

The bands I’ve had the pleasure to play with during these years; *B.D.F.O.S.*, *Joe and the Hornets*, and *Mr. Pam with Friends*, and all amazing dancers in the international Lindy Hop community. Thanks for being awesome and helping me retain a balance between my right and left brain.

Jonas, Charlie, Peter, David, Jessimaca, Stina, and Sanna. You mean so much to me – I would not have been able to complete this work without you.

My family for *always* supporting me and believing in me.

9. Summary in Swedish

Förfinade bildtagnings- och bildbehandlingsmetoder i kombination med ökad datorkraft har banat väg för sofistikerade kirurgiplaneringssystem. Sådana system har stor potential att hjälpa kirurger uppnå bättre resultat för patienten, såväl funktionellt som estetiskt, och dessutom avsevärt förkorta tiden i operationssalen vilket medför kostnadsbesparingar. Dagens planeringssystem är dock svåranvända, och många kirurger förlitar sig på externa experter under planeringsprocessen, vilket innebär längre tid till operation, och ökade kostnader.

Haptik är läran om känselsinnet, och *haptisk teknik* innefattar algoritmer, mjukvara och hårdvara med syfte att stimulera känselsinnet. För att demonstrera hur haptisk teknik i kombination med stereovisualisering kan förbättra användbarheten och effektiviteten vid planering av kirurgi, beskriver den här avhandlingen utvecklingen av systemet haptics-assisted surgery planning (HASP). Systemet stöder planering av komplexa traumafall där kirurgen ofta ställs inför en utmaning som påminner om att lösa ett komplicerat tredimensionellt pussel med stora krav på precision och noggrannhet. Systemet stöder även planering av rekonstruktioner som omfattar benvävnad, kärl och mjukvävnad i onkologiska fall. Vi testar systemet med hjälp av kirurger som på egen hand, efter en kort övningssession, får planera ett retrospektivt traumafall och fyra retrospektiva onkologiska fall. Potentialen hos HASP sträcker sig långt bortom denna avhandling och kommer förhoppningsvis att komma till användning som test- och utvecklingsplattform för framtida forskning.

För övning av kirurgisk bensågning beskriver vi en simulator med ett haptiskt hybridinterface som på ett realistiskt sätt kombinerar lågfrekventa kontaktkrafter med högfrekventa vibrationer då en virtuell såg kommer i kontakt med en virtuell benmodell.

För halvautomatisk inpassning av frakturerade virtuella objekt beskriver vi en stabil attraktionskraftsmodell, *snap-to-fit*, anpassad för integrering med etablerade haptikrenderingsmetoder för sex frihetsgrader, och med en kvasi-statisk virtuell koppling.

Vi utvärderar hur visuo-haptisk co-lokalisering påverkar genomförandetid och noggrannhet hos interaktionsuppgifter utförda på två visuo-haptiska system: ett som bygger på ett holografiskt optiskt element och ett som bygger på en halv-transparent spegel. Vi finner att hos våra uppgifter där noggrannhet, inte kort genomförandetid, är målet, ökar inte co-lokalisering noggrannheten. Däremot medför co-lokalisering en signifikant förkortning av genomförandetiden hos vår manipuleringsuppgift där genomförande på kort tid är målet.

Slutligen presenterar vi design och utvärdering av två haptiska gränssnitt avsedda att bäras på handen, drivna av två olika typer av integrerade piezoelektriska motorer: en ”walking quasi-static motor”, och en ”traveling-wave ultrasonic motor”. Den kvasi-statiska motorn fungerar bäst för haptiska tillämpningar med höga krav på precision, och där hastigheten är relativt låg. För tillämpningar som kräver högre hastigheter är den ultrasoniska motorn ett bättre alternativ.

10. Bibliography

1. Fisher, B., Fels, S., MacLean, K., Munzner, T., and Rensink, R. "Seeing, Hearing, and Touching: Putting It All Together," *ACM SIGGRAPH Course Notes*, p. 8, 2004.

2. Wang, D., Xiao, J., and Zhang, Y., *Haptic Rendering for Simulation of Fine Manipulation*. Springer, Berlin Heidelberg, 2014.

3. Sutherland, I.E. "The Ultimate Display," *Proceedings of the IFIP Congress*, 1965.

4. Klatzky, R.L. and Lederman, S.J., *Touch*. Handbook of Psychology. Wiley, New York, vol. 4, pp. 147-176, 2003.

5. Johansson, R.S. and Flanagan, J.R., "Coding and Use of Tactile Signals from the Fingertips in Object Manipulation Tasks," *Nature Reviews Neuroscience*, vol. 10, no. 5, pp. 345-359, 2009.

6. Choi, S. and Kuchenbecker, K.J., "Vibrotactile Display: Perception, Technology, and Applications," *Proceedings of the IEEE*, vol. 101, no. 9, pp. 2093-2104, 2013.

7. Johansson, R.S. and Vallbo, Å.B., "Tactile Sensibility in the Human Hand: Relative and Absolute Densities of Four Types of Mechanoreceptive Units in Glabrous Skin," *Journal of Physiology*, vol. 286, no. 1, pp. 283-300, 1979.

8. Edin, B.B. and Johansson, N., "Skin Strain Patterns Provide Kinaesthetic Information to the Human Central Nervous System," *The Journal of Physiology*, vol. 487, no. 1, pp. 243-251, 1995.

9. Edin, B.B. and Abbs, J.H., "Finger Movement Responses of Cutaneous Mechanoreceptors in the Dorsal Skin of the Human Hand," *Journal of Neurophysiology*, vol. 65, no. 3, pp. 657-670, 1991.

10. Vallbo, Å.B., Hagbarth, K.E., and Wallin, B.G., "Microneurography: How the Technique Developed and Its Role in the Investigation of the Sympathetic Nervous System," *Journal of Applied Physiology*, vol. 96, no. 4, pp. 1262-1269, 2004.

11. Stone, R.J., "Haptic Feedback: A Brief History from Telepresence to Virtual Reality," in *Haptic Human-Computer Interaction*, Springer, Berlin Heidelberg, pp. 1-16, 2001.

12. Benali-Khoudja, M., Hafez, M., Alexandre, J.-M., and Kheddar, A. "Tactile Interfaces: A State-of-the-Art Survey," *International Symposium on Robotics*, Paris, France, 2004.

13. Carignan, C.R. and Cleary, K.R., "Closed-Loop Force Control for Haptic Simulation of Virtual Environments," *Haptics-e*, vol. 1, no. 2, pp. 1-14, 2000.

14. Hannaford, B. and Okamura, A.M., "Haptics," in *Springer Handbook of Robotics*, Springer, Berlin Heidelberg, pp. 719-739, 2008.

15. Van der Linde, R.Q., Lammertse, P., Frederiksen, E., and Ruiter, B. "The Hapticmaster, a New High-Performance Haptic Interface," *Proceedings of the IEEE Eurohaptics Conference*, pp. 1-5, 2002.

16. Massie, T.H., *Design of a Three Degree of Freedom Force-Reflecting Haptic Interface*, Bachelor Thesis, Massachusetts Institute of Technology, 1993.

17. http://www.geomagic.com/.

18. Faure, F., et al., "Sofa: A Multi-Model Framework for Interactive Physical Simulation," in *Soft Tissue Biomechanical Modeling for Computer Assisted Surgery*, Springer, Berlin Heidelberg, pp. 283-321, 2012.

19. Salisbury, K., Conti, F., and Barbagli, F., "Haptic Rendering: Introductory Concepts," *IEEE Computer Graphics and Applications*, vol. 24, no. 2, pp. 24-32, 2004.

20. Palmerius, K.L., Cooper, M., and Ynnerman, A., "Haptic Rendering of Dynamic Volumetric Data," *IEEE Transactions on Visualization and Computer Graphics*, vol. 14, no. 2, pp. 263-276, 2008.

21. Otaduy, M.A. and Lin, M.C., "High Fidelity Haptic Rendering," *Synthesis Lectures on Computer Graphics and Animation*, vol. 1, no. 1, pp. 1-112, 2006.

22. Mark, W.R., Randolph, S.C., Finch, M., Van Verth, J.M., and Taylor II, R.M. "Adding Force Feedback to Graphics Systems: Issues and Solutions," *Proceedings of the 23rd Annual Conference on Computer Graphics and Interactive Techniques*, ACM, pp. 447-452, 1996.

23. http://www.sensegraphics.com/.

24. http://www.chai3d.org/.

25. Zilles, C.B. and Salisbury, J.K. "A Constraint-Based God-Object Method for Haptic Display," *Proceedings of the IEEE International Conference on Intelligent Robots and Systems*, pp. 146-151, 1995.

26. Ruspini, D.C., Kolarov, K., and Khatib, O. "The Haptic Display of Complex Graphical Environments," *Proceedings of the 24th Annual Conference on Computer Graphics and Interactive Techniques*, pp. 345-352, 1997.

27. McNeely, W.A., Puterbaugh, K.D., and Troy, J.J. "Six Degree-of-Freedom Haptic Rendering Using Voxel Sampling," *Proceedings of the 26th Annual Conference on Computer Graphics and Interactive Techniques*, pp. 401-408, 1999.

28. Barbic, J., *Real-Time Reduced Large-Deformation Models and Distributed Contact for Computer Graphics and Haptics*, PhD Thesis, Carnegie Mellon University, 2007.

29. Borgefors, G., "On Digital Distance Transforms in Three Dimensions," *Computer Vision and Image Understanding*, vol. 64, no. 3, pp. 368-376, 1996.

30. Wan, M. and McNeely, W.A. "Quasi-Static Approximation for 6 Degrees-of-Freedom Haptic Rendering," *Proceedings of the 14th IEEE Visualization Conference*, IEEE Computer Society, p. 34, 2003.

31. Okamura, A.M., Richard, C., and Cutkosky, M., "Feeling Is Believing: Using a Force-Feedback Joystick to Teach Dynamic Systems," *Journal of Engineering Education*, vol. 91, no. 3, pp. 345-349, 2002.

32. Endo, T., et al., "Five-Fingered Haptic Interface Robot: Hiro III," *IEEE Transactions on Haptics*, vol. 4, no. 1, pp. 14-27, 2011.

33. Najdovski, Z., Nahavandi, S., and Fukuda, T., "Design, Development, and Evaluation of a Pinch–Grasp Haptic Interface," *IEEE/ASME Transactions on Mechatronics*, vol. 19, no. 1, pp. 45-54, 2014.

34. Curie, J. and Curie, P., "Développement, Par Pression, De L'électricité Polaire Dans Les Cristaux Hémièdres À Faces Inclinées," *Comptes Rendus*, vol. 91, pp. 294-295, 1880.

35. Choi, B.H. and Choi, H.R., "A Semi-Direct Drive Hand Exoskeleton Using Ultrasonic Motor," *Proceedings of the IEEE International Workshop on Robot and Human Interaction*, pp. 285-290, 1999.

36. Flueckiger, M., Bullo, M., Chapuis, D., Gassert, R., and Perriard, Y., "FMRI Compatible Haptic Interface Actuated with Traveling Wave Ultrasonic Motor," *Proceedings of the Industry Applications Conference*, vol. 3, pp. 2075-2082 Vol. 3, 2005.

37. Sashida, T. and Kenjo, T., *Introduction to Ultrasonic Motors*. Oxford Univ. Press, New York, 1993.

38. http://www.piezomotor.com/.

39. Krebs, H.I., Hogan, N., Aisen, M.L., and Volpe, B.T., "Robot-Aided Neurorehabilitation," *IEEE Transactions on Rehabilitation Engineering*, vol. 6, no. 1, pp. 75-87, 1998.

40. Seth, A., Su, H.J., and Vance, J.M. "Sharp: A System for Haptic Assembly and Realistic Prototyping," *International Design Engineering Technical Conferences and Computers and Information in Engineering Conference*, American Society of Mechanical Engineers, pp. 905-912, 2006.

41. McDonnell, K.T. and Qin, H., "Virtual Clay: Haptics-Based Deformable Solids of Arbitrary Topology," in *Articulated Motion and Deformable Objects*, Springer, Berlin Heidelberg, pp. 1-20, 2002.

42. Hua, J., Duan, Y., and Qin, H. "Design and Manipulation of Polygonal Models in a Haptic, Stereoscopic Virtual Environment," *International Conference on Shape Modeling and Applications*, IEEE, pp. 145-154, 2005.

43. Orozco, M., El Saddik, A., Petriu, E., and Silva, J., *The Role of Haptics in Games*. INTECH Open Access Publisher, 2012.

44. Coles, T., Meglan, D., and John, N.W., "The Role of Haptics in Medical Training Simulators: A Survey of the State of the Art," *IEEE Transactions on Haptics*, vol. 4, no. 1, pp. 51-66, 2011.

45. Gallagher, A.G. and O'Sullivan, G.C., *Fundamentals of Surgical Simulation; Principles & Practices*. Springer, London, 2012.

46. Ullrich, S. and Kuhlen, T., "Haptic Palpation for Medical Simulation in Virtual Environments," *IEEE Transactions on Visualization and Computer Graphics*, vol. 18, no. 4, pp. 617-625, 2012.

47. Panait, L., Akkary, E., Bell, R.L., Roberts, K.E., Dudrick, S.J., and Duffy, A.J., "The Role of Haptic Feedback in Laparoscopic Simulation Training," *Journal of Surgical Research*, vol. 1, p. 5, 2009.

48. DiMaio, S.P. and Salcudean, S.E., "Interactive Simulation of Needle Insertion Models," *IEEE Transactions on Biomedical Engineering*, vol. 52, no. 7, pp. 1167-1179, 2005.

49. Forsslund, J., Chan, S., Salisbury, K.J., Silva, R.G., Girod, S., and Blevins, N.H. "Design and Implementation of a Maxillofacial Surgery Rehearsal Environment with Haptic Interaction for Bone Fragment and Plate Alignment," *International Journal of Computer Assisted Radiology and Surgery*, 2012.

50. Petersson, F. and Åkerlund, C., *Haptic Force Feedback Interaction for Planning in Maxillo-Facial Surgery*, Master Thesis, Linköping University, 2003.

51. Kovler, I., et al., "Haptic Computer-Assisted Patient-Specific Preoperative Planning for Orthopedic Fractures Surgery," *International Journal of Computer Assisted Radiology and Surgery*, pp. 1-12, 2015.

52. Jansson, G. and Monaci, L., "Haptic Identification of Objects with Different Numbers of Fingers," in *Touch, Blindness and Neurscience*, UNED Press, Madrid, pp. 203-213, 2004.

53. Ang, Q.-Z., Horan, B., Najdovski, Z., and Nahavandi, S. "Grasping Virtual Objects with Multi-Point Haptics," *Proceedings of the IEEE Virtual Reality Conference*, pp. 189-190, 2011.

54. Wang, S., Li, J., and Zheng, R., "A Resistance Compensation Control Algorithm for a Cable-Driven Hand Exoskeleton for Motor Function Rehabilitation," in *Intelligent Robotics and Applications*, Springer, Berlin Heidelberg, pp. 398-404, 2010.

55. http://www.cyberglovesystems.com/.

56. Bouzit, M., Burdea, G., Popescu, G., and Boian, R., "The Rutgers Master Ii-New Design Force-Feedback Glove," *IEEE/ASME Transactions on Mechatronics*, vol. 7, no. 2, pp. 256-263, 2002.

57. Solomon, C. and Breckon, T., *Fundamentals of Digital Image Processing: A Practical Approach with Examples in Matlab*. John Wiley & Sons, 2011.

58. Bartlett, M.S., Movellan, J.R., and Sejnowski, T.J., "Face Recognition by Independent Component Analysis," *IEEE Transactions on Neural Networks*, vol. 13, no. 6, pp. 1450-1464, 2002.

59. Wahlberg, F., Dahllöf, M., Mårtensson, L., and Brun, A., "Spotting Words in Medieval Manuscripts," *Studia Neophilologica*, vol. 86, no. 1, pp. 171-186, 2014.

60. Gurcan, M.N., Boucheron, L.E., Can, A., Madabhushi, A., Rajpoot, N.M., and Yener, B., "Histopathological Image Analysis: A Review," *IEEE Reviews in Biomedical Engineering*, vol. 2, pp. 147-171, 2009.

61. Veta, M., Pluim, J.P., van Diest, P.J., and Viergever, M., "Breast Cancer Histopathology Image Analysis: A Review," *IEEE Transactions on Biomedical Engineering* vol. 61, no. 5, pp. 1400-1411, 2014.

62. Kylberg, G., Uppström, M., Hedlund, K.O., Borgefors, G., and Sintorn, I.M., "Segmentation of Virus Particle Candidates in Transmission Electron Microscopy Images," *Journal of Microscopy*, vol. 245, no. 2, pp. 140-147, 2012.

63. Lidayová, K., Frimmel, H., Wang, C., Bengtsson, E., and Smedby, Ö., "Fast Vascular Skeleton Extraction Algorithm," *Pattern Recognition Letters*, 2015.

64. Nysjö, J., Malmberg, F., Sintorn, I.M., and Nyström, I., "Bonesplit - a 3d Texture Painting Tool for Interactive Bone Separation in Ct Images," *Journal of WSCG*, vol. 23, no. 1-2, pp. 157-166, 2015.

65. Friman, O., Hindennach, M., and Peitgen, H.O. "Template-Based Multiple Hypotheses Tracking of Small Vessels," *IEEE International Symposium on Biomedical Imaging: From Nano to Macro*, Paris, France, 2008.

66. Wright, H., *Introduction to Scientific Visualization*. Springer, London, 2007.

67. Held, R.T. and Hui, T.T., "A Guide to Stereoscopic 3d Displays in Medicine," *Academic Radiology*, vol. 18, no. 8, pp. 1035-1048, 2011.

68. Zachow, S., Gladilin, E., Trepczynski, A., Sader, R., and Zeilhofer, H.F., "3d Osteotomy Planning in Cranio-Maxillofacial Surgery: Experiences and Results of Surgery Planning and Volumetric Finite-Element Soft Tissue Prediction in Three Clinical Cases," in *Proceedings of Computer Assisted Radiology and Surgery*, pp. 983-987, 2002.

69. May, P., "A Survey of 3-D Display Technologies," *Journal of Information Display*, vol. 32, pp. 28-33, 2005.

70. Gustafsson, J., Lindfors, C., Mattsson, L., and Kjellberg, T. "Large-Format 3d Interaction Table," *Conference on Stereoscopic Display and Virtural Reality Systems XII*, San Jose, USA, International Society for Optics and Photonics, pp. 589-595, 2005.

71. Holliman, N.S., Dodgson, N., Favalora, G.E., and Pockett, L., "Three-Dimensional Displays: A Review and Applications Analysis," *IEEE Transactions on Broadcasting*, vol. 57, no. 2, pp. 362-371, 2011.

72. Van Schooten, B., Van Dijk, E., Zudilova Seinstra, E., Suinesiaputra, A., and Reiber, J. "The Effect of Stereoscopy and Motion Cues on 3d Interpretation Task Performance," *Proceedings of the International Conference on Advanced Visual Interfaces*, pp. 167-170, 2010.

73. Ware, C. and Mitchell, P., "Visualizing Graphs in Three Dimensions," *ACM Transactions on Applied Perception*, vol. 5, no. 1, p. 2, 2008.

74. http://www.naturalpoint.com/.

75. Olsson, P., Nysjö, F., Seipel, S., and Carlbom, I. "Physically Co-Located Haptic Interaction with 3d Displays," *Proceedings of the IEEE Haptics Symposium*, pp. 267-272, 2012.

76. Teather, R.J., Allison, R.S., and Stuerzlinger, W., *Evaluating Visual/Motor Co-Location in Fish-Tank Virtual Reality*, in *Science and Technology for Humanity* 2009: Toronto, Canada. pp. 624-629.

77. Groen, J. and Werkhoven, P.J., "Visuomotor Adaptation to Virtual Hand Position in Interactive Virtual Environments," *Presence: Teleoperators and Virtual Environments*, vol. 7, no. 5, pp. 429-446, 1998.

78. http://www.devinsense.com/.

79. Boyle, P. and Levin, B., *World Cancer Report 2008*. IARC Press, International Agency for Research on Cancer, 2008.

80. Peden, M., *World Report on Road Traffic Injury Prevention*. World Health Organization, Geneva, 2004.

81. Ridgway, E.B. and Weiner, H.L., "Skull Deformities," *Pediatric Clinics of North America*, vol. 51, pp. 359-387, 2004.

82. Lyhne, N.M., et al., "Waiting Times for Diagnosis and Treatment of Head and Neck Cancer in Denmark in 2010 Compared to 1992 and 2002," *European Journal of Cancer*, vol. 49, no. 7, pp. 1627-33, 2013.

83. Roser, S.M., et al., "The Accuracy of Virtual Surgical Planning in Free Fibula Mandibular Reconstruction: Comparison of Planned and Final Results," *Journal of Oral and Maxillofacial Surgery*, vol. 68, no. 11, pp. 2824-32, 2010.

84. Leiggener, C.S., Krol, Z., Gawelin, P., Buitrago-Tellez, C.H., Zeilhofer, H.F., and Hirsch, J.M., "A Computer-Based Comparative Quantitative Analysis of Surgical Outcome of Mandibular Reconstructions with Free Fibula Microvascular Flaps," *Journal of Plastic Surgery and Hand Surgery*, vol. 49, no. 2, pp. 95-101, 2014.

85. Roser, S.M., et al., "The Accuracy of Virtual Surgical Planning in Free Fibula Mandibular Reconstruction: Comparison of Planned and Final Results," *Journal of Oral and Maxillofacial Surgery*, vol. 68, no. 11, pp. 2824-2832, 2010.

86. Antony, A.K., Chen, W.F., Kolokythas, A., Weimer, K.A., and Cohen, M.N., "Use of Virtual Surgery and Stereolithography-Guided Osteotomy for Mandibular Reconstruction with the Free Fibula," *Plastic and Reconstructive Surgery*, vol. 128, no. 5, pp. 1080-1084, 2011.

87. Zweifel, D.F., Simon, C., Hoarau, R., Pasche, P., and Broome, M., "Are Virtual Planning and Guided Surgery for Head and Neck Reconstruction Economically Viable?," *Journal of Oral and Maxillofacial Surgery*, vol. 73, no. 1, pp. 170-175, 2015.

88. Vannier, M.W., Marsh, J.L., and Warren, J.O. "Three Dimensional Computer Graphics for Craniofacial Surgical Planning and Evaluation," *ACM SIGGRAPH*, pp. 263-273, 1983.

89. http://www.brainlab.com/.

90. http://www.materialise.com/.

91. Huotilainen, E., et al., "Inaccuracies in Additive Manufactured Medical Skull Models Caused by the Dicom to STL Conversion Process," *Journal of Cranio-Maxillofacial Surgery*, vol. 42, no. 5, pp. 259-265, 2014.

92. Brown, B.J., et al. "A System for High-Volume Acquisition and Matching of Fresco Fragments: Reassembling Theran Wall Paintings," *ACM Transactions on Graphics*, p. 84, 2008.

93. Huang, Q.X., Flöry, S., Gelfand, N., Hofer, M., and Pottmann, H., "Reassembling Fractured Objects by Geometric Matching," *ACM Transactions on Graphics*, vol. 25, no. 3, pp. 569-578, 2006.

94. Besl, P.J. and McKay, N.D. "Method for Registration of 3-D Shapes," *Robotics-DL tentative*, International Society for Optics and Photonics, pp. 586-606, 1992.

95. Mellado, N., Reuter, P., and Schlick, C. "Semi-Automatic Geometry-Driven Reassembly of Fractured Archeological Objects," *Proceedings of the 11th International Symposium on Virtual Reality, Archaeology and Cultural Heritage*, pp. 33-38, 2010.

96. Hidalgo, D.A., "Fibula Free Flap: A New Method of Mandible Reconstruction," *Plastic and Reconstructive Surgergy*, vol. 84, no. 1, pp. 71-9, 1989.

97. Wei, F.C., Chen, H.C., Chuang, C.C., and Noordhoff, M.S., "Fibular Osteoseptocutaneous Flap: Anatomic Study and Clinical Application," *Plastic and Reconstructive Surgery*, vol. 78, no. 2, pp. 191-199, 1986.

98. Yua, D., Zhengb, X., Chenc, M., and Shend, S.G., "Preliminarily Measurement and Analysis of Sawing Forces in Fresh Cadaver Mandible Using Reciprocating Saw for Reality-Based Haptic Feedback," *Journal of Craniofacial Surgery*, vol. 23, no. 3, pp. 925-929, 2012.

99. Morris, D., Sewell, C., Barbagli, F., Salisbury, K., Blevins, N.H., and Girod, S., "Visuohaptic Simulation of Bone Surgery for Training and Evaluation," *IEEE Compututer Graphics and Applications*, vol. 26, pp. 48-57, 2006.

100. Weik, M., "Nyquist Theorem," in *Computer Science and Communications Dictionary*, Springer US, p. 1127, 2001.

101. http://www.tactilelabs.com/.

102. Bexell, M. and Johansson, S., "Fabrication and Evaluation of a Piezoelectric Miniature Motor," *Sensors and Actuators A: Physical*, vol. 75, no. 1, pp. 8-16, 1999.

103. http://www.piezo-tech.com/.

104. Maples, J. and Becke, J.J., "Experiments in Force Control of Robotic Manipulators," *Proc. IEEE Int'l Conf. Robotics and Automation*, vol. 3, pp. 695-702, 1986.

All websites were successfully accessed on September 16, 2015.

Acta Universitatis Upsaliensis

Digital Comprehensive Summaries of Uppsala Dissertations from the Faculty of Science and Technology 1289

Editor: The Dean of the Faculty of Science and Technology

A doctoral dissertation from the Faculty of Science and Technology, Uppsala University, is usually a summary of a number of papers. A few copies of the complete dissertation are kept at major Swedish research libraries, while the summary alone is distributed internationally through the series Digital Comprehensive Summaries of Uppsala Dissertations from the Faculty of Science and Technology. (Prior to January, 2005, the series was published under the title "Comprehensive Summaries of Uppsala Dissertations from the Faculty of Science and Technology".)

Distribution: publications.uu.se
urn:nbn:se:uu:diva-262378

ACTA
UNIVERSITATIS
UPSALIENSIS
UPPSALA
2015